
ScatterAD: Temporal-Topological Scattering Mechanism for Time Series Anomaly Detection

Tao Yin¹ Xiaohong Zhang^{1*} Shaochen Fu¹ Zhibin Zhang¹ Li Huang¹
 Yiyuan Yang² Kaixiang Yang³ Meng Yan^{1*}

¹Chongqing University ²University of Oxford ³South China University of Technology

{yintao, fushaochen}@stu.cqu.edu.cn, {xhongz, zbinz, lee.h, mengy}@cqu.edu.cn
 yiyuan.yang@cs.ox.ac.uk, yangkx@scut.edu.cn

Abstract

One main challenge in time series anomaly detection for industrial IoT lies in the complex spatio-temporal couplings within multivariate data. However, traditional anomaly detection methods focus on modeling spatial or temporal dependencies independently, resulting in suboptimal representation learning and limited sensitivity to anomalous dispersion in high-dimensional spaces. In this work, we conduct an empirical analysis showing that both normal and anomalous samples tend to scatter in high-dimensional space, especially anomalous samples are markedly more dispersed. We formalize this dispersion phenomenon as scattering, quantified by the mean pairwise distance among sample representations, and leverage it as an inductive signal to enhance spatio-temporal anomaly detection. Technically, we propose ScatterAD to model representation scattering across temporal and topological dimensions. ScatterAD incorporates a topological encoder for capturing graph-structured scattering and a temporal encoder for constraining over-scattering through mean squared error minimization between neighboring time steps. We introduce a contrastive fusion mechanism to ensure the complementarity of the learned temporal and topological representations. Additionally, we theoretically show that maximizing the conditional mutual information between temporal and topological views improves cross-view consistency and enhances more discriminative representations. Extensive experiments on multiple public benchmarks show that ScatterAD achieves state-of-the-art performance on multivariate time series anomaly detection. Code is available at this repository: <https://github.com/jk-sounds/ScatterAD>.

1 Introduction

Multivariate time series data in Industrial Internet of Things (IoT) systems exhibit intricate spatio-temporal relationships[Tian et al., 2023], and anomaly detection is crucial to ensure the stable operation of the system[Efthymiou et al., 2018, Baraniuk, 2020]. Recognizing abnormal patterns from complex data has become a critical and widely studied problem in both research and practical domains[Mohammadi et al., 2018, Wollschlaeger et al., 2017]. However, anomalies in multivariate time series frequently manifest synergistically in temporal and topological dimensions[Jin et al., 2024, Yi et al., 2024, Zhao et al., 2024], presenting highly coupled complex characteristics, which pose a severe challenge to traditional anomaly detection methods.

*Corresponding authors.

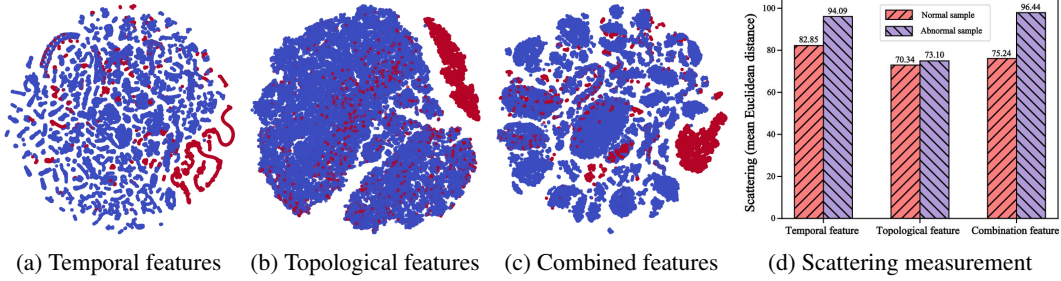


Figure 1: The distribution patterns of scatter visualization and scatter measurement in time features, topological features, and combined temporal-topological features (obtained by simple linear combination) on the SWaT dataset. Blue and red represent the embeddings of normal points and abnormal points respectively. Normal data exhibits clustering characteristics, abnormal data exhibits scattering characteristics, and combined features show more significant scattering differences. This provides a strong prior signal for anomaly detection.

Time series anomaly detection methods are broadly bifurcated into two principal categories: methods based on temporal pattern learning and methods based on topological structure modeling. Temporal pattern-based methods (such as [Park et al., 2018, Su et al., 2019, Xu et al., 2021, Wu et al., 2021]) primarily focus on the sequential dependency of time series data and identify data points that deviate from normal temporal patterns by constructing predictive or reconstructive models. However, recursive models for learning temporal patterns exhibit limitations in capturing pairwise dependencies between variables, limiting their ability to identify intricate anomalies [Zhao et al., 2020, Xu et al., 2021]. Conversely, topological structure-based methods (such as GDN [Deng and Hooi, 2021], GTAD [Guan et al., 2022], TopoGDN [Liu et al., 2024] etc.) focus on modeling the graph structure relationship between variables and detecting anomalies by learning the mutual dependence between variables. While these methodologies can model spatial correlations, they often fail to fully leverage the dynamic characteristics of time series. Methodologies focusing exclusively on either temporal or spatial patterns often prove inadequate for modeling the intricate spatio-temporal dynamics in multivariate time series, consequently leading to challenges in effectively capturing the "scattering" phenomenon of anomalies in the spatio-temporal dimension. As shown in Figure 1, we visualize the scattering patterns of temporal features, topological features, and their linear combination features on the SWaT dataset, using the average Euclidean distance to quantify the degree of scattering between samples. It is evident from the scattering representation diagram and the scattering metric diagram that the combined feature space usually exhibits more pronounced scattering differences than the temporal feature space and the topological feature space. In essence, anomaly detection is the identification of samples outside the data distribution (Out-of-distribution, OOD) [Wang et al., 2020]. Significant scattering differences can bring better anomaly separation capabilities to the model. In other words, when the scattering of anomalous samples is more pronounced, their feature representations are pushed further apart from the normal samples, creating a clearer boundary for anomaly detection. More recently, several studies have endeavored to consider both the temporal and spatial dimensions, such as MTAD-GAT [Zhao et al., 2020]. However, MTAD-GAT employ simple feature concatenation or serial processing methods and fail to address the challenge of collaborative optimization of spatio-temporal features in theory. In particular, they lack a deep understanding and modeling of the complementarity of spatio-temporal features.

The information bottleneck principle [Tishby et al., 2000] offers a theoretical framework for addressing such challenges of spatio-temporal feature complementarity. This principle aims to extract a representation Z from the input variable X , such that Z preserves maximal information as possible about the target variable Y in X , while compressing redundant information in X that is irrelevant to Y . In particular, when complementary representations need to be learned from different dimensions (such as temporal and topological), a single bottleneck objective may fail to effectively align the relationship between the representations of each dimension [Federici et al., 2020]. Considering that anomalies in multivariate time series typically manifest as abnormal scattering of spatio-temporal patterns, we propose a theoretical hypothesis: effective anomaly detection needs to capture the scattering representation characteristics of both the temporal and topological dimensions and ensure the complementarity of these two features. Through theoretical analysis, we prove that under the condition of a given graph

structure G , maximizing the mutual information $I(Z_T; Z_G | G)$ between the temporal representation Z_T and the topological representation Z_G can facilitate effective anomaly detection. This theoretical result can be expressed as: $\max I(Z_T; Z_G | G)$ s.t. $I(X, Z_T) < r_1, I(X, Z_G) < r_2$, where r_1 and r_2 control the compression degree of the temporal and topological representations respectively. This shows that, subject to the constraint that the temporal and topological representations are fully compressed, maximizing their conditional mutual information can promote the synergistic complementarity of the two representations, thereby improving the performance of anomaly detection.

Specifically, we propose a novel anomaly detection approach ScatterAD, which enables effective representation learning of spatio-temporal representation through three principal mechanisms: first, the scattering mechanism is designed to capture the scattering characteristics of the representation in the feature dimension in the temporal-topological representation; second, we further incorporate a time constraint mechanism to prevent excessive scattering of the representation to maintain the consistency of the temporal structure; finally, in order to align temporal and topological representations in the latent representation space, we introduce contrastive fuse mechanism to align the outputs of the temporal and topological encoders, maintaining the compression constraints while promoting the complementarity of the representations. Unlike prior work, which treats temporal and topological patterns separately, ScatterAD introduces a unified contrastive scattering mechanism that jointly optimizes temporal consistency and structural distinguishability.

The contribution of our paper is summarized as follows:

- We introduce ScatterAD, a novel anomaly detection approach that employs a temporal-topological scattering mechanism to improve representational discriminability while preserving temporal structural consistency.
- To the best of our knowledge, this is the first work to introduce information bottleneck theory into multivariate time series anomaly detection, to theoretically reveal the complementarity between temporal and topological features. This leads to more discriminative representations and highlights the importance of integrating spatio-temporal information in future anomaly detection research.
- Extensive experiments conducted on six public benchmark datasets and using twelve standard evaluation metrics demonstrate that ScatterAD achieves state-of-the-art performance, validating both the theoretical foundations and practical effectiveness of our design.

2 Related Work

Anomaly Detection in Time Series Given the scarcity and imbalance of data labels, unsupervised anomaly detection methods have received widespread attention in recent years [Choi et al., 2021]. Primarily focused on the reconstruction error-driven autoencoder model [Kingma et al., 2013], or its probabilistic extension, the variational autoencoder [Su et al., 2019]. These methods capture local reconstruction patterns but struggle to capture fine-scale dependencies and dynamic propagation across time points. Graph neural networks (GNNs) have been introduced to model the dependency structure between different variables in multivariate time series. Representative methods such as MTGNN [Wu et al., 2020] and GDN [Deng and Hooi, 2021] typically regard each variable as a node in the graph and introduce graph convolution to learn spatial structure. However, these methods focus on spatial graph modeling between variables, neglecting the temporal graph structure. Consequently, they depend on topological associations between variables and have limited capacity to model the time dimension. More recently, several studies have initiated the exploration of graph structures in the time dimension. For instance, GANF [Dai and Chen, 2022] and MTGFlow [Zhou et al., 2023] construct time series graph structures and combine density modeling methods to model the distribution of the entire sequence, but these methods still do not deeply explore the structural characteristics and interdependencies between time nodes. Although methods such as TopoGDN [Liu et al., 2024] and CST-GL [Zheng et al., 2023] model spatio-temporal dependencies, they overlook representation scattering in high-dimensional spaces, which can potentially impede their sensitivity to the dispersion patterns characteristic of anomalies.

Information bottleneck and representation complementarity The classic information bottleneck principle [Tishby et al., 2000] explicitly articulates the objective of retaining task-relevant information while compressing redundant inputs. Based on this foundation, Deep InfoMax [Hjelm et al., 2018]

and InfoGraph [Sun et al., 2019] employ a mutual information maximization strategy to align local and global representations in structured data, including images and graphs. Models such as MVGRL [Hassani and Khasahmadi, 2020] and structured mutual information models [Yang et al., 2025] promote complementarity between different representation views, which have the potential to substantially enhance the performance of downstream tasks.

3 Method

3.1 Overview

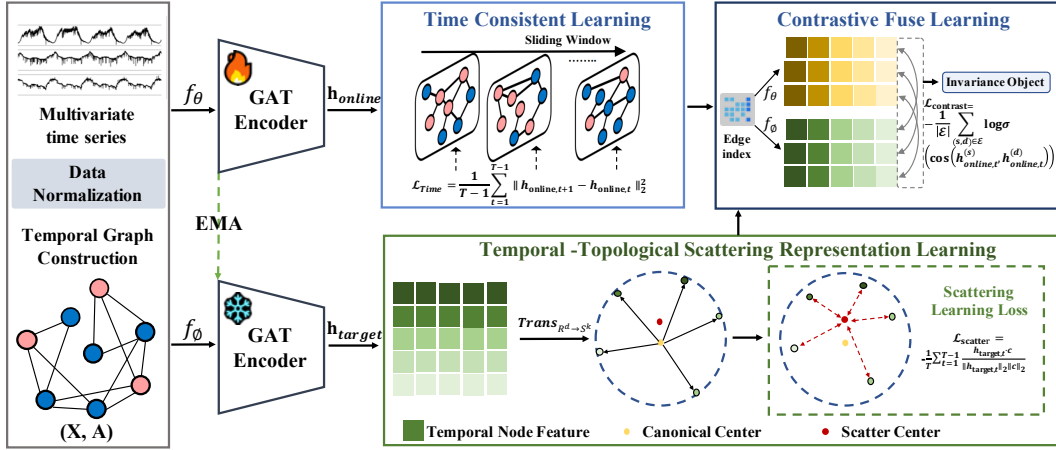


Figure 2: The overall framework of ScatterAD employs temporal graphs to model the scattering patterns of nodes in multivariate time series. It encodes temporal nodes as graph vertices to capture structural scattering, constrains time consistency to avoid excessive scattering, and aligns temporal topological features through contrastive fusion, ultimately achieving effective detection through scattering representation learning.

As illustrated in Figure 2, ScatterAD employs an online encoder $f_\theta(\cdot)$ and a target encoder $f_\phi(\cdot)$ to process the temporal graph G , where θ and ϕ denote the parameters of the respective encoders. (1) A topological space is initially defined via L_2 -normalizing node features onto the unit hypersphere, with a global scatter center c randomly initialized inside the unit ball (see Section 3.3 for details). Following the positive-only sampling strategy used in DCdetector [Yang et al., 2023], all training samples are treated as positive samples. Within this embedding space, the target encoder $f_\phi(\cdot)$ learns to model the compactness of normal samples, thereby capturing scattering representations and amplifying the scattering of anomalous samples during inference. (2) The online encoder $f_\theta(\cdot)$ yields h_{online} and enforces temporal smoothness via a temporal constraint on adjacent temporal nodes, preventing excessive scattering in the target encoder $f_\phi(\cdot)$. Only the online encoder is updated via backpropagation; the target encoder parameters ϕ are updated using the exponential moving average (EMA) of the online encoder parameters θ after each training step (see Section 3.2 for details). (3) The online and target encoders constitute a contrastive fusion framework to maximize the similarity between them, thereby fostering collaboration between the online and target encoders. (4) Regarding the anomaly judgment criterion, anomalies are evaluated based on scattering deviation and time consistency deviation (see Section 3.3 for details).

The definition of multivariate time series anomaly detection is as follows: Let $\mathcal{X} = \{x_t\}_{t=1}^T$, $\mathcal{X} \in \mathbb{R}^{T \times N}$ be a multivariate time series with N dimensions and a sliding window length of T , $x_t = [x_t^1, x_t^2, \dots, x_t^N]^\top \in \mathbb{R}^N$ represent the N -dimensional observation vector at time t , and the sequence length is T . The goal of anomaly detection is to predict the anomaly label $\mathcal{Y}_t \in \{0, 1\}$ for each timestamp t , where $\mathcal{Y}_t = 1$ indicates that time t is in an abnormal state, and $\mathcal{Y}_t = 0$ indicates a normal state.

3.2 Temporal Graph Construction and Node Feature Extraction

Our framework employs a dual-encoder architecture to learn temporally and topologically aggregated representations of normal patterns at temporal nodes. Unlike prior graph-based time series models, where each node corresponds to a sensor or univariate stream, we consider each time step as a distinct node. Specifically, each graph node represents a multidimensional time slice $x_t \in \mathbb{R}^N$, and the edge set is defined as $\mathcal{E} = (v_{t-k}, v_t) \mid k \in [1, \tau], t \in [\tau + 1, T]$, capturing the behavioral patterns across time through directed connections. Here, τ is the look-back window size. In our experiments, we set $\tau = 2$. To extract temporal dynamics from the input sequence, we apply a multi-scale causal convolutional encoder. Let $h^{(0)} = \mathcal{X}$ denote the input time series:

$$h^{(l)} = \text{PReLU} \left(\mathcal{BN} \left(\sum_{i=0}^{k-1} \mathcal{W}_c^{(i)} \cdot h_{t-i}^{(l-1)} \right) \right), \quad \text{for } t = k, \dots, T, \quad (1)$$

where $\mathcal{W}_c^{(i)}$ denotes the i -th convolution kernel in a k -length causal convolution, $\mathcal{BN}(\cdot)$ signifies batch normalization [Ioffe and Szegedy, 2015]. To further integrate topological dependencies across temporal nodes, we employ a multi-head GAT layer to compute attention coefficients across nodes:

$$\alpha_{ij}^h = \frac{\exp(\text{LeakyReLU}(a_h^\top [\mathcal{W}_h h_i \| \mathcal{W}_h h_j]))}{\sum_{k \in \mathcal{N}_i} \exp(\text{LeakyReLU}(a_h^\top [\mathcal{W}_h h_i \| \mathcal{W}_h h_k]))}, \quad (2)$$

α_{ij}^h denotes the normalized attention coefficients of the h -th head. $h_i, h_j \in h^{(l)}$ represent the input feature vectors of nodes i and j . \mathcal{W}_h is the head-specific parameter matrix and the a_h^\top is the attention coefficient vector.

$$h'_i = \text{ELU} \left(\bigoplus_{h=1}^H \left(\sum_{j \in \mathcal{N}_i} \text{softmax} \left(a_{ij}^{(h)} \right) \mathcal{W}_h h_j \right) \right). \quad (3)$$

Subsequently, the node features are aggregated with topological features and temporal features, yielding $z_i = h'_i + h^{(l)}$. $z_i \in \mathbb{R}^{T \times d_{out}}$ denotes the stacked temporal and topological representations.

3.3 Optimization Target

Time Consistent Learning The loss of time consistency is introduced to node features $z_{\text{online},t} \in z_i$ to reinforce the temporal dependency of adjacent nodes and prevent them from excessive dispersion in the feature subspace, thereby preserving the key temporal features of the nodes. The formulation is as follows:

$$\mathcal{L}_{\text{time}} = \frac{1}{T-1} \sum_{t=1}^{T-1} \|z_{\text{online},t+1} - z_{\text{online},t}\|_2^2, \quad (4)$$

here, each row $z_{\text{online},t} \in \mathbb{R}^{d_{out}}$ corresponds to the node representation at time step t and $\mathcal{L}_{\text{time}}$ penalizes abrupt representation shifts between consecutive encoding states.

Temporal Topological Scattering Representation Learning We propose a graph scattering mechanism to explicitly guide the target encoder in learning decentralized representations of nodes. For node representation, we initially define a regular subspace \mathbb{S}^k and a scattering center c . For the subspace \mathbb{S}^k , a transformation function $\text{Trans}(\cdot)$ is employed to transform the representation from the original space \mathbb{R}^d to \mathbb{S}^k . Specifically, we apply L_2 -normalizing to each row vector z_i within the matrix $z_{\text{target},t}$:

$$\tilde{z}_{\text{target},t} = \text{Trans}_{\mathbb{R}^d \rightarrow \mathbb{S}^k}(z_{\text{target},t}) = \frac{z_{\text{target},t}}{\|z_{\text{target},t}\|_2}, \quad \mathbb{S}^k = \{\tilde{z}_{\text{target},t} : \|\tilde{z}_{\text{target},t}\|_2 = 1\}, \quad (5)$$

where $\tilde{z}_{\text{target},t} \in \mathbb{S}^k$ is the target representation on the unit sphere (normalized), as defined in the formula, the representations of all nodes are distributed in the hypersphere \mathbb{S}^k . This mapping prevents arbitrary scattering of representations in the space, thereby mitigating instability and optimization difficulties during training. Afterwards, we initialize a global scattering center, c , which serves as a fixed anchor point within the latent space. This center is randomly sampled to reside strictly

inside the unit hypersphere. The initialization is a two-step process: first, an intermediate vector \mathbf{c}' is sampled from a standard multivariate normal distribution. Second, this vector is L2-normalized to project it onto the unit hypersphere and then scaled by a random scalar $\epsilon \in (0, 1)$. This procedure can be formally expressed as: $\mathbf{c}' \sim \mathcal{N}(0, I)$, $\mathbf{c} = \frac{\mathbf{c}'}{\|\mathbf{c}'\|_2} \cdot \epsilon$, where $\epsilon \sim \mathcal{U}(0, 1)$. With this fixed scattering center \mathbf{c} , we then introduce the representation scattering loss, L_{scatter} , designed to pull the representations of normal samples towards it:

$$\mathcal{L}_{\text{scatter}} = -\frac{1}{T} \sum_{t=1}^T \frac{\tilde{z}_{\text{target},t}^\top \cdot \mathbf{c}}{\|\tilde{z}_{\text{target},t}\|_2 \|\mathbf{c}\|_2}. \quad (6)$$

By maximizing this loss function, the learned target features remain close to the semantic center while preserving directional diversity, which is crucial for amplifying the scattering behavior of anomalous nodes during inference.

Contrastive Fuse Learning To ensure that the nodes maintain consistent directions in both the embedding space and the projected hypersphere space, while preserving local structures and global geometric properties. We maximize the similarity between positive sample pairs from both encoders, thereby ensuring that the embedding space preserves local structural relationships while the scattering space maintains global node relationships. The formulation is as follows:

$$\mathcal{L}_{\text{contrast}} = -\frac{1}{|\mathcal{E}|} \sum_{(s,d) \in \mathcal{E}} \log \sigma \left(\cos \left(z_{\text{online},t}^{(s)} \cdot z_{\text{target},t}^{(d)} \right) \right). \quad (7)$$

Here, \mathcal{E} denotes the set of edges of graph and σ is the sigmoid activation function, (s, d) representing the origin and terminus of the corresponding edge, constituting a positive sample pair, $z_{\text{online},t}^{(s)}$ and $z_{\text{target},t}^{(d)}$ denote the feature vectors generated by the encoder $f_\theta(\cdot)$ and the encoder $f_\phi(\cdot)$.

Exponential Moving Average Mechanism During the training process, the parameters θ of the online encoder are updated via gradient descent, and the parameters ϕ are updated through the Exponential Moving Average mechanism [Cai et al., 2021] by the online encoder. Compared with direct alignment constraints and centralized representations, the prediction target serves as a buffer mechanism, enabling the target encoder to adaptively learn local time constraint information and global topological scattering representation. The exponential moving average mechanism is applied at the end of each training epoch. The formula is as follows:

$$\theta \leftarrow m\theta + (1 - m)\xi. \quad (8)$$

Among them, $(0 < m < 1)$, this process facilitates the integration of graph time structure consistency into the node scattering representation process, effectively alleviating the confrontation brought about by direct optimization of alignment constraints and decentralized representations. Representation scattering is used to enhance the global distinguishability of information, and time consistency loss ensures the consistency of local information. The interaction of these two mechanisms enables the target encoder to learn global topological scattering features more stably while preserving local temporal information.

Loss Function The overall training objective of ScatterAD integrates three loss components:

$$\mathcal{L}_{\text{total}} = \mathcal{L}_{\text{scatter}} + \mathcal{L}_{\text{time}} + \mathcal{L}_{\text{contrast}}, \quad (9)$$

$\mathcal{L}_{\text{scatter}}$ captures the scattering representation by modeling the compactness of normal samples within the topological space, thereby implicitly amplifying the contrast with anomalous patterns and enhancing feature discriminability. $\mathcal{L}_{\text{time}}$ enforces time consistency by penalizing abrupt changes between adjacent time steps, mitigating over-scattering. $\mathcal{L}_{\text{contrast}}$ aligns temporal and topological representations through a cross-view contrastive loss based on cosine similarity, fostering their complementarity. This joint optimization encourages the model to learn discriminative, temporally consistent, and cross-view complementary representations for robust anomaly detection.

3.4 Anomaly Criterion

To jointly evaluate anomalies from both the topological scattering and time consistency perspectives, we define a unified anomaly scoring function that captures two complementary forms of deviation.

For the anomaly score of the input sequence \mathcal{X} , it is initially transformed into a node representation $z_i = f_\theta(\mathcal{X})$, $z_i \in \mathbb{R}^{N \times d_{out}}$. The scattering deviation score $\mathcal{D}(\mathcal{X})$, which quantifies how far the target node representation deviates from the learned center in the normalized representation space, and the time inconsistency score $\mathcal{L}(\mathcal{X})$, which penalizes abrupt representation shifts between consecutive time steps. The ultimate anomaly score is formulated as follows:

$$\text{AnomalyScore}(\mathcal{X}) = \underbrace{\mathcal{D}(\mathcal{X}) : \frac{1}{\min_k \mathcal{D}(z_i, c)}}_{\text{Scattering deviation}} + \underbrace{\mathcal{L}(\mathcal{X}) : \frac{1}{d} \sum_{i=1}^d (z_i^{(t)} - z_i^{(t-1)})^2}_{\text{Time inconsistency}}. \quad (10)$$

This is a point-level anomaly detection approach, where anomalous points are expected to receive higher anomaly scores. Following prior work [Xu et al., 2021, Yang et al., 2023], we introduce a threshold δ to convert scores into binary labels: a point is labeled as anomalous ($y = 1$) if its score exceeds δ , and normal ($y = 0$) otherwise.

4 Experiments

4.1 Experimental Setup

Datasets

We conducted evaluations on six real-world multivariate time series datasets, including **(1) PSM** (Pooled Server Metrics)[Abdulaal et al., 2021]; **(2) MSL** (Mars Science Laboratory)[Hundman et al., 2018]; **(3) SWaT**(Secure Water Treatment)[Mathur and Tippenhauer, 2016]; **(4) WADI** (Water Distribution)[Ahmed et al., 2017]; **(5) NIPS-TS-SWAN**[Lai et al., 2021]; **(6) NIPS-TS-GECCO**[Lai et al., 2021]. See Appendix B for dataset details and statistics.

Metrics We evaluate detection performance using both label-based and score-based metrics. For label-based metrics, we report the point-adjusted F1 score (PA-F), which considers an anomaly segment detected if any timestamp within it is flagged. Although it may overestimate performance, it is widely used [Xu et al., 2021, Guan et al., 2022, Song et al., 2023]. To ensure fair comparisons, we also report the Affiliated F1 score (Aff-F) [Huet et al., 2022], which measures alignment quality between predicted and ground-truth anomaly segments. Additionally, we include score-based metrics: Area under the ROC Curve (A-ROC) [Fawcett, 2006] and Area under the Precision-Recall Curve (A-PR)[Boyd et al., 2013]. In summation, we report results across twelve evaluation metrics, with comprehensive reports detailed reports in Appendix C.

Baselines We compare our method against a diverse set of baselines, including recent state-of-the-art graph-based and transformer-based models: Sub-Adjacent Transformer (S.T.)[Yue et al., 2024], TopoGDN (T.G.)[Liu et al., 2024], Memto [Song et al., 2023], DuoGAT (D.G.)[Lee et al., 2023], MTGFlow (MTG)[Zhou et al., 2023], iTTransformer (iT.)[Liu et al., 2023], DCdetector (DC.)[Yang et al., 2023], Anomaly Transformer (A.T.][Xu et al., 2021], and GANF[Dai and Chen, 2022]. We also include classical methods such as ModernTCN (M.TCN)[Luo and Wang, 2024], Variational Autoencoder (VAE)[Pinheiro Cinelli et al., 2021], Isolation Forest (IF)[Liu et al., 2008], and PCA [Shyu et al., 2003] for a comprehensive evaluation.

4.2 Main Results

We evaluate ScatterAD on six real-world multivariate time series datasets utilizing four standard evaluation metrics: Affiliated-F1 (Aff-F), Point-Adjusted-F1 (PA-F), AUC-ROC (A-ROC), and AUC-PR (A-PR). As demonstrated in Table 1, ScatterAD consistently achieves the best performance, ranking first in 15 out of 24 evaluation settings. Notably, ScatterAD achieves the highest Affiliated-F1 scores across all datasets, demonstrating its superior ability to localize anomalies at the segment level. While performance on the NIPS-TS-SWAN (N-T-S) dataset is mixed, with the highest scores in PA-F (0.736), A-ROC (0.792), and A-PR (0.716), but a notably low Aff-F (0.038), we attribute this to the irregular and bursty nature of anomalies in the dataset, which makes segment-level matching particularly challenging. Nonetheless, the robust Point-Adjusted-F1 suggests robust detection capabilities under noisy and complex conditions. Furthermore, ScatterAD consistently achieves the highest AUC-ROC values across all datasets, indicating a strong trade-off between true positive and false positive rates under varying threshold settings.

Table 1: Performance comparison on six real-world datasets. Evaluation Metrics: Aff-F (affiliated F1), PA-F (point-adjusted F1), A-ROC (AUC-ROC), and A-PR (AUC-PR). Higher values indicate better performance. All reported results are averaged over multiple independent runs to ensure robustness. **Bold** indicates the optimal performance; Underline indicates the suboptimal performance.

Dataset	Metric	Ours	S.T.	T.G.	Memto	DC.	M.TCN	IT.	MTG	A.T.	D.G.	GANF	VAE	IF	PCA
MSL	Aff-F	0.867	0.673	0.674	0.595	0.674	<u>0.709</u>	0.652	0.374	0.673	0.677	0.323	0.642	0.374	0.591
	PA-F	0.964	0.863	0.714	0.664	<u>0.947</u>	0.807	0.659	0.648	0.934	0.652	0.489	0.512	0.598	0.444
	A-ROC	0.986	0.751	0.794	0.951	0.961	0.627	0.604	0.857	<u>0.970</u>	0.788	0.678	0.883	0.673	0.732
	A-PR	0.932	0.754	0.727	<u>0.902</u>	0.891	0.739	0.721	0.781	0.878	0.703	0.620	0.521	0.519	0.524
PSM	Aff-F	0.797	0.786	0.689	0.659	0.653	0.701	0.652	0.436	0.657	0.624	0.329	0.524	0.569	0.437
	PA-F	0.981	0.941	0.801	0.977	0.977	0.965	0.926	0.797	<u>0.978</u>	0.780	0.788	0.596	0.543	0.467
	A-ROC	0.986	0.731	0.830	<u>0.981</u>	0.948	0.581	0.687	0.832	0.977	0.074	0.825	0.758	0.634	0.908
	A-PR	0.969	0.806	<u>0.965</u>	0.542	0.866	0.629	0.751	0.753	0.961	0.245	0.745	0.443	0.344	0.687
SWaT	Aff-F	0.704	0.631	0.594	0.592	0.687	0.685	0.716	0.463	0.622	0.619	0.608	0.563	0.502	0.537
	PA-F	0.951	0.863	0.788	0.756	0.939	0.884	0.916	0.500	<u>0.943</u>	0.822	0.244	0.526	0.472	0.548
	A-ROC	0.982	0.956	0.766	0.841	0.876	0.675	0.662	0.769	0.989	0.094	0.574	0.532	0.501	0.502
	A-PR	0.909	<u>0.868</u>	0.822	0.810	0.824	0.592	0.619	0.851	0.657	0.503	0.830	0.432	0.511	0.421
WADI	Aff-F	0.605	0.756	0.532	0.701	<u>0.725</u>	0.558	0.671	0.673	0.708	0.636	0.667	0.556	0.555	0.477
	PA-F	0.862	0.873	0.834	0.807	0.731	0.766	0.754	0.690	0.738	0.705	0.681	0.512	0.474	0.618
	A-ROC	0.960	0.945	0.612	0.693	0.829	0.831	0.814	0.782	0.982	0.372	0.782	0.501	0.860	0.502
	A-PR	0.765	0.743	0.532	0.691	0.651	0.697	0.627	0.523	0.637	0.470	0.508	0.384	0.406	0.357
NIPS-TS-SWAN	Aff-F	0.038	0.805	0.685	0.033	0.484	0.533	0.507	0.003	0.099	0.659	0.005	0.385	0.438	0.680
	PA-F	0.736	0.714	0.660	0.687	<u>0.733</u>	0.731	0.729	0.591	0.695	0.503	0.630	0.497	0.522	0.526
	A-ROC	0.792	0.870	0.595	0.791	0.655	0.562	0.537	0.788	0.787	0.671	0.778	0.522	0.729	0.498
	A-PR	0.716	0.946	0.527	0.702	0.626	0.545	0.531	0.699	0.569	0.714	0.712	0.326	0.473	0.326
NIPS-TS-GECCO	Aff-F	0.825	0.476	0.589	0.424	0.648	0.446	0.435	0.348	0.658	<u>0.667</u>	0.268	0.481	0.531	0.509
	PA-F	0.784	0.491	0.670	0.504	0.472	0.357	0.381	0.381	0.325	0.625	0.355	0.491	0.481	0.583
	A-ROC	0.969	0.536	0.787	0.875	0.715	0.946	0.817	0.732	0.685	0.690	0.898	0.868	0.684	0.763
	A-PR	0.633	0.318	0.495	0.519	0.523	0.615	0.474	0.552	0.870	0.535	0.337	0.443	0.418	0.543
#1 Count		15	4	0	0	0	0	1	0	3	0	0	0	0	0

Figure 3 illustrates anomaly score distributions on SWaT. As shown in Figures 3a- 3c, competing methods exhibit significant overlap between normal and anomalous scores, limiting detection precision. In contrast, ScatterAD (Figure 3d) exhibits a clear separation, and the anomaly scores for normal points are sharply concentrated near zero, while anomalies are widely spread across higher scores, forming multiple distinguishable modes. This distinct gap between normal and anomalous distributions greatly reduces the false positive rate and enhances detection precision.

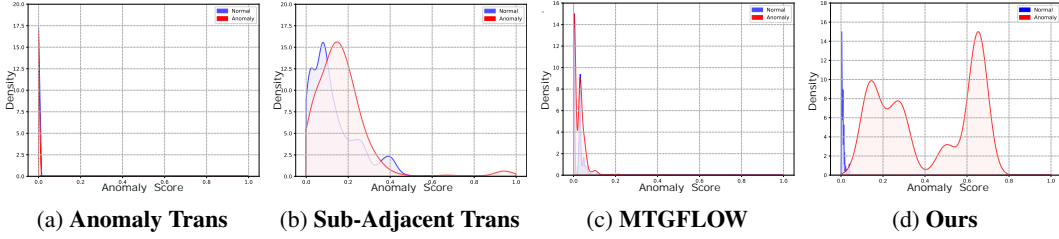


Figure 3: The distribution of anomaly scores presented by different frameworks on the SWaT dataset.

4.3 Ablation Studies

To validate the effectiveness of ScatterAD’s components, we conduct an ablation study on its dual encoder architecture and contrastive fusion mechanism (Table 2). Removing the temporal online encoder (“w/o T-Enc”) impairs the model’s ability to capture temporal variations, reducing detection performance. Excluding the topological target encoder (“w/o S-Enc”) leads to significant drops, particularly on WADI and SWaT, underscoring the need to model global structural dependencies. Eliminating the contrastive fusion module (“w/o C-Fuse”) results in consistent performance degradation across all datasets, confirming its importance in aligning temporal and topological cues. Removing the Exponential Moving Average mechanism (“w/o EMA”) destabilizes target encoder updates, degrading performance by limiting adaptation to temporal and structural patterns.

Table 2: Ablation analysis of key components of ScatterAD across four real-world datasets. Evaluation Metrics: AF (Affiliated-F1), AR (Area Under the ROC Curve). **Bold** indicates the optimal performance; Underline indicates the suboptimal performance.

Variation	MSL		PSM		WADI		SWaT		#1 Count
	AF	AR	AF	AR	AF	AR	AF	AR	
w/o T-Enc	0.764	0.927	0.810	0.951	<u>0.568</u>	<u>0.958</u>	0.659	0.944	1
w/o S-Enc	<u>0.841</u>	0.963	<u>0.799</u>	<u>0.985</u>	0.488	0.921	0.643	0.974	0
w/o C-Fuse	0.795	0.932	0.788	0.946	0.549	0.953	<u>0.701</u>	<u>0.975</u>	0
w/o EMA	0.805	0.986	0.792	0.979	0.582	0.955	0.683	0.957	1
ScatterAD	0.867	<u>0.983</u>	0.794	0.986	0.587	0.960	0.704	0.982	6

4.4 Model Analysis

Analysis of Scattering Mechanism To validate our hypothesis that dynamically balancing scattering and structure consistency enables learning node representations with both discriminability and temporal dependency, we analyze the evolution of scattering during training (Figure 4). When using only the time consistency loss $\mathcal{L}_{\text{time}}$ 4a, the heat map shows smooth but low-amplitude scattering, indicating strong temporal continuity but limited anomaly sensitivity. In contrast, using only the scattering loss $\mathcal{L}_{\text{scatter}}$ 4b increases node dispersion and discriminability but disrupts temporal coherence. Our full method 4c, which combines $\mathcal{L}_{\text{time}}$, $\mathcal{L}_{\text{scatter}}$ and $\mathcal{L}_{\text{contrast}}$, achieves a balanced scattering pattern that preserves structure while enhancing anomaly separability. Compared to single-loss variants, it yields more stable training and more effective representations for temporal anomaly detection.

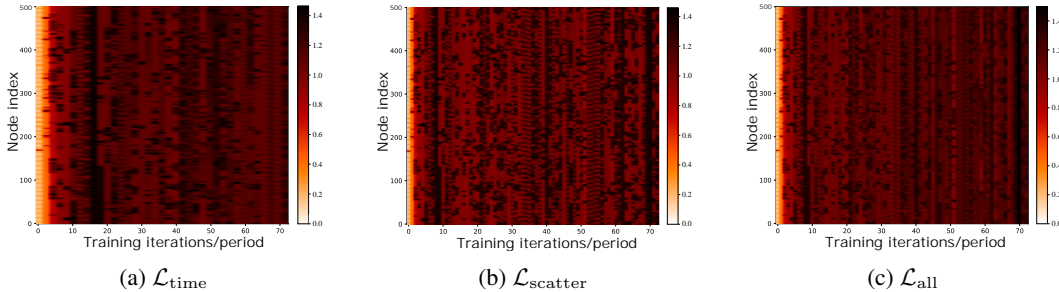


Figure 4: Scattering of different time nodes during training on the MSL dataset, measured by the average Euclidean distance between sample representations. (a) Optimized with only $\mathcal{L}_{\text{time}}$. (b) Optimized with only $\mathcal{L}_{\text{scatter}}$. (c) Our method. Darker colors indicate nodes with greater average distances from others. Compared to (a) and (b), our loss function preserves temporal dependencies while promoting more discriminative node representations during training.

Analysis of Latent Discrepancy in Layer-Wise Evolution The embedding space transforms significantly across GAT layers, as shown in Figures 5. Initially, normal and anomalous sample embeddings are entangled (Figure 5a). After passing through the GAT layers (Figures 5b and 5c), a structured separation emerges. Normal sample embeddings form cohesive clusters, while anomalous ones scatter outwards. This progression reveals that our model effectively increases the inter-class embedding discrepancy. Rather than explicitly enforcing a margin-based separation, the model implicitly learns to emphasize this discrepancy by capturing richer spatio-temporal interactions through attention mechanisms. This behavior aligns with our notion of spatio-temporal scattering, wherein the joint modeling of temporal dynamics and variable interdependencies causes anomalies to naturally drift away from the normal data manifold in the representation space. Crucially, by amplifying the dissimilarity between normal and anomalous embeddings in both local neighborhoods and global structure, the model enhances its sensitivity to out-of-distribution (OOD) patterns.

Analysis of Anomaly Criteria Figure 6 visually compares the anomaly scores of different methods. Our approach demonstrates superior detection across various anomaly types compared to baselines. Specifically, MTGFlow suffers from high false positives, while AnomalyTrans has noticeable false negatives. Sub-Adjacent Trans, despite detecting all anomaly types, also generates significant false

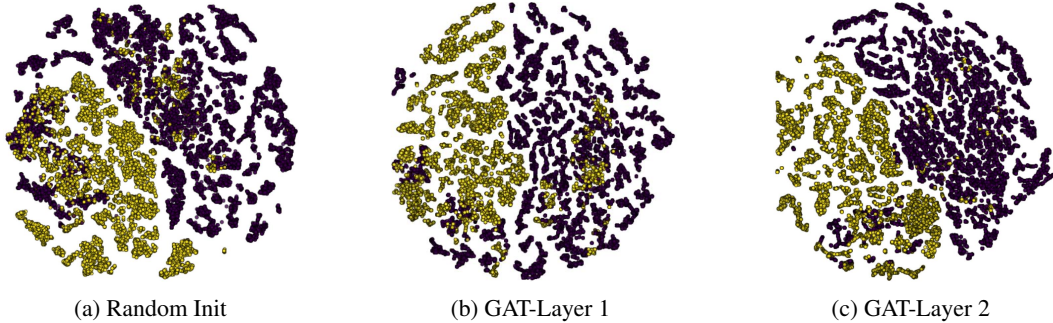


Figure 5: t-SNE embeddings of GAT on the PSM dataset. Blue and yellow dots denote perturbed negative and positive samples, respectively. The embeddings evolve from an initial entangled state to increasingly disentangled clusters in deeper encoder layers.

alarms, particularly for contextual and shapelet anomalies, where it incorrectly assigns high scores to normal regions. In contrast, our method not only highlights anomalies more effectively but also reduces false positives, leading to improved accuracy and robustness.

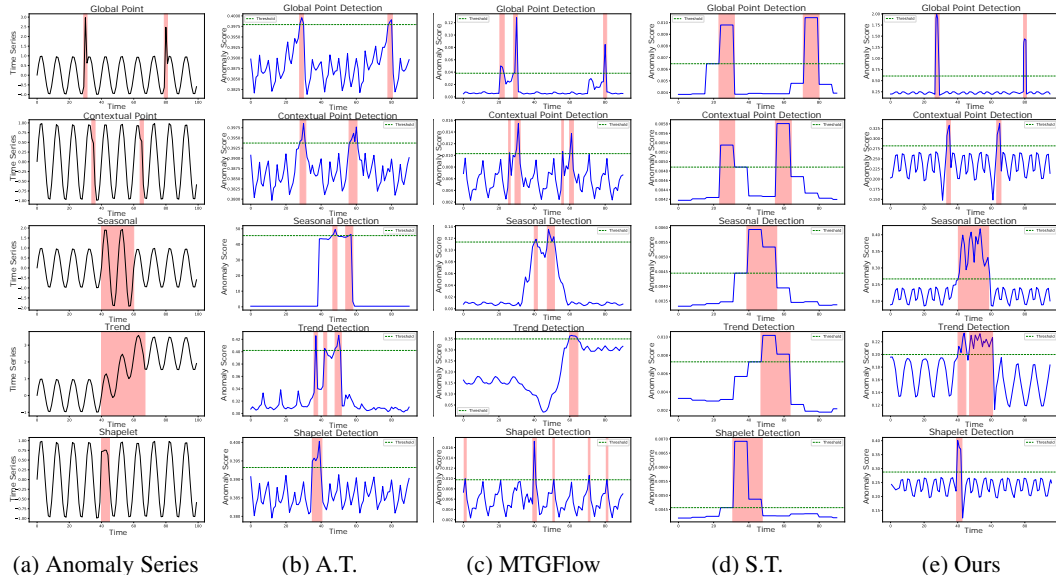


Figure 6: Visualization comparison of ground truth anomalies and anomaly scores across different types. The pink segments are marked as anomalies of the pattern.

5 Conclusion

In this work, we propose ScatterAD, a novel approach integrating topological and temporal contrastive learning. ScatterAD enhances the discriminability of representations through a scattering mechanism, followed by the application of a topological constraint mechanism to prevent over-scattering and maintain temporal consistency, and introduces a contrastive fusion strategy to foster the synergistic complementarity of temporal and topological representations to improve anomaly detection performance. Comprehensive experimentation demonstrates that ScatterAD attains strong performance across diverse benchmarks. The proposed temporal and topological representation fusion mechanism significantly improves the model’s ability to distinguish normal and anomalous patterns, providing valuable insights for developing more effective anomaly detection systems.

6 Acknowledgments

This work is supported by the National Key Research and Development Project of China (No. 2024YFB3309900), the Fundamental Research Funds for the Central Universities (No. 2025CDJZKKYJH-08), the National Natural Science Foundation of China (No. 62476101), the Chongqing Technology Innovation and Application Development Project (No. CSTB2023TIAD-STX0025), and the Guangdong Basic and Applied Basic Research Foundation (No. 2024A1515140137).

References

Ahmed Abdulaal, Zhuanghua Liu, and Tomer Lancewicki. Practical approach to asynchronous multivariate time series anomaly detection and localization. In *Proceedings of the 27th ACM SIGKDD conference on knowledge discovery & data mining*, pages 2485–2494, 2021.

Chuadhy Mujeeb Ahmed, Venkata Reddy Palleti, and Aditya P Mathur. Wadi: a water distribution testbed for research in the design of secure cyber physical systems. In *Proceedings of the 3rd international workshop on cyber-physical systems for smart water networks*, pages 25–28, 2017.

C Baraniuk. Tracking down three billion litres of lost water. *BBC News*, 2020.

Kendrick Boyd, Kevin H Eng, and C David Page. Area under the precision-recall curve: point estimates and confidence intervals. In *Machine Learning and Knowledge Discovery in Databases: European Conference, ECML PKDD 2013, Prague, Czech Republic, September 23-27, 2013, Proceedings, Part III 13*, pages 451–466. Springer, 2013.

Zhaowei Cai, Avinash Ravichandran, Subhransu Maji, Charless Fowlkes, Zhuowen Tu, and Stefano Soatto. Exponential moving average normalization for self-supervised and semi-supervised learning. In *Proceedings of the IEEE/CVF conference on computer vision and pattern recognition*, pages 194–203, 2021.

Kukjin Choi, Jihun Yi, Changhwa Park, and Sungroh Yoon. Deep learning for anomaly detection in time-series data: Review, analysis, and guidelines. *IEEE access*, 9:120043–120065, 2021.

Enyan Dai and Jie Chen. Graph-augmented normalizing flows for anomaly detection of multiple time series. *arXiv preprint arXiv:2202.07857*, 2022.

Ailin Deng and Bryan Hooi. Graph neural network-based anomaly detection in multivariate time series. In *Proceedings of the AAAI conference on artificial intelligence*, volume 35, pages 4027–4035, 2021.

Marina Efthymiou, Eric Tchouamou Njoya, Pak Lam Lo, Andreas Papatheodorou, and Daniel Randall. The impact of delays on customers’ satisfaction: An empirical analysis of the british airways on-time performance at heathrow airport. *Journal of Aerospace Technology and Management*, 11: e0219, 2018.

Tom Fawcett. An introduction to roc analysis. *Pattern recognition letters*, 27(8):861–874, 2006.

Marco Federici, Anjan Dutta, Patrick Forré, Nate Kushman, and Zeynep Akata. Learning robust representations via multi-view information bottleneck. *arXiv preprint arXiv:2002.07017*, 2020.

Siwei Guan, Binjie Zhao, Zhekang Dong, Mingyu Gao, and Zhiwei He. Gtd: Graph and temporal neural network for multivariate time series anomaly detection. *Entropy*, 24(6):759, 2022.

Kaveh Hassani and Amir Hosein Khasahmadi. Contrastive multi-view representation learning on graphs. In *International conference on machine learning*, pages 4116–4126. PMLR, 2020.

R Devon Hjelm, Alex Fedorov, Samuel Lavoie-Marchildon, Karan Grewal, Phil Bachman, Adam Trischler, and Yoshua Bengio. Learning deep representations by mutual information estimation and maximization. *arXiv preprint arXiv:1808.06670*, 2018.

Alexis Huet, Jose Manuel Navarro, and Dario Rossi. Local evaluation of time series anomaly detection algorithms. In *Proceedings of the 28th ACM SIGKDD Conference on Knowledge Discovery and Data Mining*, pages 635–645, 2022.

Kyle Hundman, Valentino Constantinou, Christopher Laporte, Ian Colwell, and Tom Soderstrom. Detecting spacecraft anomalies using lstms and nonparametric dynamic thresholding. In *Proceedings of the 24th ACM SIGKDD international conference on knowledge discovery & data mining*, pages 387–395, 2018.

Sergey Ioffe and Christian Szegedy. Batch normalization: Accelerating deep network training by reducing internal covariate shift. In *International conference on machine learning*, pages 448–456. pmlr, 2015.

Ming Jin, Huan Yee Koh, Qingsong Wen, Daniele Zambon, Cesare Alippi, Geoffrey I Webb, Irwin King, and Shirui Pan. A survey on graph neural networks for time series: Forecasting, classification, imputation, and anomaly detection. *IEEE Transactions on Pattern Analysis and Machine Intelligence*, 2024.

Diederik P Kingma, Max Welling, et al. Auto-encoding variational bayes, 2013.

Kwei-Herng Lai, Daochen Zha, Junjie Xu, Yue Zhao, Guanchu Wang, and Xia Hu. Revisiting time series outlier detection: Definitions and benchmarks. In *Thirty-fifth conference on neural information processing systems datasets and benchmarks track (round 1)*, 2021.

Jongsoo Lee, Byeongtae Park, and Dong-Kyu Chae. Duogat: Dual time-oriented graph attention networks for accurate, efficient and explainable anomaly detection on time-series. In *Proceedings of the 32nd ACM International Conference on Information and Knowledge Management*, pages 1188–1197, 2023.

Fei Tony Liu, Kai Ming Ting, and Zhi-Hua Zhou. Isolation forest. In *2008 eighth ieee international conference on data mining*, pages 413–422. IEEE, 2008.

Qinghua Liu and John Paparrizos. The elephant in the room: Towards a reliable time-series anomaly detection benchmark. *Advances in Neural Information Processing Systems*, 37:108231–108261, 2024.

Yong Liu, Tengge Hu, Haoran Zhang, Haixu Wu, Shiyu Wang, Lintao Ma, and Mingsheng Long. itransformer: Inverted transformers are effective for time series forecasting. *arXiv preprint arXiv:2310.06625*, 2023.

Zhe Liu, Xiang Huang, Jingyun Zhang, Zhifeng Hao, Li Sun, and Hao Peng. Multivariate time-series anomaly detection based on enhancing graph attention networks with topological analysis. In *Proceedings of the 33rd ACM International Conference on Information and Knowledge Management*, pages 1555–1564, 2024.

Donghao Luo and Xue Wang. Moderntcn: A modern pure convolution structure for general time series analysis. In *The twelfth international conference on learning representations*, pages 1–43, 2024.

Aditya P Mathur and Nils Ole Tippenhauer. Swat: A water treatment testbed for research and training on ics security. In *2016 international workshop on cyber-physical systems for smart water networks (CySWater)*, pages 31–36. IEEE, 2016.

Mehdi Mohammadi, Ala Al-Fuqaha, Sameh Sorour, and Mohsen Guizani. Deep learning for iot big data and streaming analytics: A survey. *IEEE Communications Surveys & Tutorials*, 20(4):2923–2960, 2018.

Aaron van den Oord, Yazhe Li, and Oriol Vinyals. Representation learning with contrastive predictive coding. *arXiv preprint arXiv:1807.03748*, 2018.

John Paparrizos, Paul Boniol, Themis Palpanas, Ruey S Tsay, Aaron Elmore, and Michael J Franklin. Volume under the surface: a new accuracy evaluation measure for time-series anomaly detection. *Proceedings of the VLDB Endowment*, 15(11):2774–2787, 2022.

Daehyung Park, Yuuna Hoshi, and Charles C Kemp. A multimodal anomaly detector for robot-assisted feeding using an lstm-based variational autoencoder. *IEEE Robotics and Automation Letters*, 3(3):1544–1551, 2018.

Lucas Pinheiro Cinelli, Matheus Araújo Marins, Eduardo Antônio Barros da Silva, and Sérgio Lima Netto. Variational autoencoder. In *Variational methods for machine learning with applications to deep networks*, pages 111–149. Springer, 2021.

Ben Poole, Sherjil Ozair, Aaron Van Den Oord, Alex Alemi, and George Tucker. On variational bounds of mutual information. In *International conference on machine learning*, pages 5171–5180. PMLR, 2019.

Mei-Ling Shyu, Shu-Ching Chen, Kanoksri Sarinnapakorn, and LiWu Chang. A novel anomaly detection scheme based on principal component classifier. In *Proceedings of the IEEE foundations and new directions of data mining workshop*, pages 172–179. IEEE Press Piscataway, NJ, USA, 2003.

Junho Song, Keonwoo Kim, Jeonglyul Oh, and Sungzoon Cho. Memto: Memory-guided transformer for multivariate time series anomaly detection. *Advances in Neural Information Processing Systems*, 36:57947–57963, 2023.

Ya Su, Youjian Zhao, Chenhao Niu, Rong Liu, Wei Sun, and Dan Pei. Robust anomaly detection for multivariate time series through stochastic recurrent neural network. In *Proceedings of the 25th ACM SIGKDD international conference on knowledge discovery & data mining*, pages 2828–2837, 2019.

Fan-Yun Sun, Jordan Hoffmann, Vikas Verma, and Jian Tang. Infograph: Unsupervised and semi-supervised graph-level representation learning via mutual information maximization. *arXiv preprint arXiv:1908.01000*, 2019.

Zhiwen Tian, Ming Zhuo, Leyuan Liu, Junyi Chen, and Shijie Zhou. Anomaly detection using spatial and temporal information in multivariate time series. *Scientific Reports*, 13(1):4400, 2023.

Naftali Tishby, Fernando C Pereira, and William Bialek. The information bottleneck method. *arXiv preprint physics/0004057*, 2000.

Ziyu Wang, Bin Dai, David Wipf, and Jun Zhu. Further analysis of outlier detection with deep generative models. *Advances in Neural Information Processing Systems*, 33:8982–8992, 2020.

Martin Wollschlaeger, Thilo Sauter, and Juergen Jasperneite. The future of industrial communication: Automation networks in the era of the internet of things and industry 4.0. *IEEE industrial electronics magazine*, 11(1):17–27, 2017.

Yulei Wu, Hong-Ning Dai, and Haina Tang. Graph neural networks for anomaly detection in industrial internet of things. *IEEE Internet of Things Journal*, 9(12):9214–9231, 2021.

Zonghan Wu, Shirui Pan, Guodong Long, Jing Jiang, Xiaojun Chang, and Chengqi Zhang. Connecting the dots: Multivariate time series forecasting with graph neural networks. In *Proceedings of the 26th ACM SIGKDD international conference on knowledge discovery & data mining*, pages 753–763, 2020.

Jiehui Xu, Haixu Wu, Jianmin Wang, and Mingsheng Long. Anomaly transformer: Time series anomaly detection with association discrepancy. *arXiv preprint arXiv:2110.02642*, 2021.

Hanzhe Yang, Youlong Wu, Dingzhu Wen, Yong Zhou, and Yuanming Shi. Structured ib: Improving information bottleneck with structured feature learning. In *Proceedings of the AAAI Conference on Artificial Intelligence*, volume 39, pages 21922–21928, 2025.

Yiyuan Yang, Chaoli Zhang, Tian Zhou, Qingsong Wen, and Liang Sun. Dcdetector: Dual attention contrastive representation learning for time series anomaly detection. In *Proceedings of the 29th ACM SIGKDD Conference on Knowledge Discovery and Data Mining*, pages 3033–3045, 2023.

Shuang Yi, Sheng Zheng, Senquan Yang, Guangrong Zhou, and Jiajun Cai. Anomaly detection for asynchronous multivariate time series of nuclear power plants using a temporal-spatial transformer. *Sensors*, 24(9):2845, 2024.

Wenzhen Yue, Xianghua Ying, Ruohao Guo, DongDong Chen, Ji Shi, Bowei Xing, Yuqing Zhu, and Taiyan Chen. Sub-adjacent transformer: improving time series anomaly detection with reconstruction error from sub-adjacent neighborhoods. *arXiv preprint arXiv:2404.18948*, 2024.

Hang Zhao, Yujing Wang, Juanyong Duan, Congrui Huang, Defu Cao, Yunhai Tong, Bixiong Xu, Jing Bai, Jie Tong, and Qi Zhang. Multivariate time-series anomaly detection via graph attention network. In *2020 IEEE international conference on data mining (ICDM)*, pages 841–850. IEEE, 2020.

Mengmeng Zhao, Haipeng Peng, Lixiang Li, and Yeqing Ren. Multivariate time series anomaly detection based on spatial-temporal network and transformer in industrial internet of things. *Computers, Materials & Continua*, 80(2), 2024.

Yu Zheng, Huan Yee Koh, Ming Jin, Lianhua Chi, Khoa T Phan, Shirui Pan, Yi-Ping Phoebe Chen, and Wei Xiang. Correlation-aware spatial-temporal graph learning for multivariate time-series anomaly detection. *IEEE Transactions on Neural Networks and Learning Systems*, 35(9): 11802–11816, 2023.

Qihang Zhou, Jiming Chen, Haoyu Liu, Shibo He, and Wenchao Meng. Detecting multivariate time series anomalies with zero known label. In *Proceedings of the AAAI Conference on Artificial Intelligence*, volume 37, pages 4963–4971, 2023.

NeurIPS Paper Checklist

1. Claims

Question: Do the main claims made in the abstract and introduction accurately reflect the paper's contributions and scope?

Answer: **[Yes]**

Justification: The abstract and introduction of this paper clearly state our main contributions: We propose a novel multivariate time series anomaly detection method, ScatterAD. All claims are supported by empirical experiments in Section 4 and theoretical analysis in Appendix C, and are verified on a range of public industrial IoT datasets and tasks.

Guidelines:

- The answer NA means that the abstract and introduction do not include the claims made in the paper.
- The abstract and/or introduction should clearly state the claims made, including the contributions made in the paper and important assumptions and limitations. A No or NA answer to this question will not be perceived well by the reviewers.
- The claims made should match theoretical and experimental results, and reflect how much the results can be expected to generalize to other settings.
- It is fine to include aspirational goals as motivation as long as it is clear that these goals are not attained by the paper.

2. Limitations

Question: Does the paper discuss the limitations of the work performed by the authors?

Answer: **[Yes]**

Justification: The limitations of ScatterAD are discussed in Appendix K, including dependency on graph construction quality, the assumption of static topology, and lack of explicit causality modeling.

Guidelines:

- The answer NA means that the paper has no limitation while the answer No means that the paper has limitations, but those are not discussed in the paper.
- The authors are encouraged to create a separate "Limitations" section in their paper.
- The paper should point out any strong assumptions and how robust the results are to violations of these assumptions (e.g., independence assumptions, noiseless settings, model well-specification, asymptotic approximations only holding locally). The authors should reflect on how these assumptions might be violated in practice and what the implications would be.

- The authors should reflect on the scope of the claims made, e.g., if the approach was only tested on a few datasets or with a few runs. In general, empirical results often depend on implicit assumptions, which should be articulated.
- The authors should reflect on the factors that influence the performance of the approach. For example, a facial recognition algorithm may perform poorly when image resolution is low or images are taken in low lighting. Or a speech-to-text system might not be used reliably to provide closed captions for online lectures because it fails to handle technical jargon.
- The authors should discuss the computational efficiency of the proposed algorithms and how they scale with dataset size.
- If applicable, the authors should discuss possible limitations of their approach to address problems of privacy and fairness.
- While the authors might fear that complete honesty about limitations might be used by reviewers as grounds for rejection, a worse outcome might be that reviewers discover limitations that aren't acknowledged in the paper. The authors should use their best judgment and recognize that individual actions in favor of transparency play an important role in developing norms that preserve the integrity of the community. Reviewers will be specifically instructed to not penalize honesty concerning limitations.

3. Theory assumptions and proofs

Question: For each theoretical result, does the paper provide the full set of assumptions and a complete (and correct) proof?

Answer: **[Yes]**

Justification: We provide the theoretical analysis and complete proof in Appendix A, where we show that maximizing the conditional mutual information between temporal and topological views enhances cross-view consistency and representation discriminability.

Guidelines:

- The answer NA means that the paper does not include theoretical results.
- All the theorems, formulas, and proofs in the paper should be numbered and cross-referenced.
- All assumptions should be clearly stated or referenced in the statement of any theorems.
- The proofs can either appear in the main paper or the supplemental material, but if they appear in the supplemental material, the authors are encouraged to provide a short proof sketch to provide intuition.
- Inversely, any informal proof provided in the core of the paper should be complemented by formal proofs provided in appendix or supplemental material.
- Theorems and Lemmas that the proof relies upon should be properly referenced.

4. Experimental result reproducibility

Question: Does the paper fully disclose all the information needed to reproduce the main experimental results of the paper to the extent that it affects the main claims and/or conclusions of the paper (regardless of whether the code and data are provided or not)?

Answer: **[Yes]**

Justification: We provide all the necessary experimental details in Appendix B, including the datasets used, the specific model configurations, and the evaluation metrics. Furthermore, we make our code publicly available to ensure full reproducibility of the experimental results.

Guidelines:

- The answer NA means that the paper does not include experiments.
- If the paper includes experiments, a No answer to this question will not be perceived well by the reviewers: Making the paper reproducible is important, regardless of whether the code and data are provided or not.
- If the contribution is a dataset and/or model, the authors should describe the steps taken to make their results reproducible or verifiable.

- Depending on the contribution, reproducibility can be accomplished in various ways. For example, if the contribution is a novel architecture, describing the architecture fully might suffice, or if the contribution is a specific model and empirical evaluation, it may be necessary to either make it possible for others to replicate the model with the same dataset, or provide access to the model. In general, releasing code and data is often one good way to accomplish this, but reproducibility can also be provided via detailed instructions for how to replicate the results, access to a hosted model (e.g., in the case of a large language model), releasing of a model checkpoint, or other means that are appropriate to the research performed.
- While NeurIPS does not require releasing code, the conference does require all submissions to provide some reasonable avenue for reproducibility, which may depend on the nature of the contribution. For example
 - (a) If the contribution is primarily a new algorithm, the paper should make it clear how to reproduce that algorithm.
 - (b) If the contribution is primarily a new model architecture, the paper should describe the architecture clearly and fully.
 - (c) If the contribution is a new model (e.g., a large language model), then there should either be a way to access this model for reproducing the results or a way to reproduce the model (e.g., with an open-source dataset or instructions for how to construct the dataset).
 - (d) We recognize that reproducibility may be tricky in some cases, in which case authors are welcome to describe the particular way they provide for reproducibility. In the case of closed-source models, it may be that access to the model is limited in some way (e.g., to registered users), but it should be possible for other researchers to have some path to reproducing or verifying the results.

5. Open access to data and code

Question: Does the paper provide open access to the data and code, with sufficient instructions to faithfully reproduce the main experimental results, as described in supplemental material?

Answer: [\[Yes\]](#)

Justification: We provide open access to the data and code in Appendix B.

Guidelines:

- The answer NA means that paper does not include experiments requiring code.
- Please see the NeurIPS code and data submission guidelines (<https://nips.cc/public/guides/CodeSubmissionPolicy>) for more details.
- While we encourage the release of code and data, we understand that this might not be possible, so “No” is an acceptable answer. Papers cannot be rejected simply for not including code, unless this is central to the contribution (e.g., for a new open-source benchmark).
- The instructions should contain the exact command and environment needed to run to reproduce the results. See the NeurIPS code and data submission guidelines (<https://nips.cc/public/guides/CodeSubmissionPolicy>) for more details.
- The authors should provide instructions on data access and preparation, including how to access the raw data, preprocessed data, intermediate data, and generated data, etc.
- The authors should provide scripts to reproduce all experimental results for the new proposed method and baselines. If only a subset of experiments are reproducible, they should state which ones are omitted from the script and why.
- At submission time, to preserve anonymity, the authors should release anonymized versions (if applicable).
- Providing as much information as possible in supplemental material (appended to the paper) is recommended, but including URLs to data and code is permitted.

6. Experimental setting/details

Question: Does the paper specify all the training and test details (e.g., data splits, hyperparameters, how they were chosen, type of optimizer, etc.) necessary to understand the results?

Answer: [\[Yes\]](#)

Justification: We provide comprehensive experimental details in Appendix B.4

Guidelines:

- The answer NA means that the paper does not include experiments.
- The experimental setting should be presented in the core of the paper to a level of detail that is necessary to appreciate the results and make sense of them.
- The full details can be provided either with the code, in appendix, or as supplemental material.

7. Experiment statistical significance

Question: Does the paper report error bars suitably and correctly defined or other appropriate information about the statistical significance of the experiments?

Answer: [\[NA\]](#)

Justification: All anomaly detection results in the paper are averages under three random seeds to eliminate randomness.

Guidelines:

- The answer NA means that the paper does not include experiments.
- The authors should answer "Yes" if the results are accompanied by error bars, confidence intervals, or statistical significance tests, at least for the experiments that support the main claims of the paper.
- The factors of variability that the error bars are capturing should be clearly stated (for example, train/test split, initialization, random drawing of some parameter, or overall run with given experimental conditions).
- The method for calculating the error bars should be explained (closed form formula, call to a library function, bootstrap, etc.)
- The assumptions made should be given (e.g., Normally distributed errors).
- It should be clear whether the error bar is the standard deviation or the standard error of the mean.
- It is OK to report 1-sigma error bars, but one should state it. The authors should preferably report a 2-sigma error bar than state that they have a 96% CI, if the hypothesis of Normality of errors is not verified.
- For asymmetric distributions, the authors should be careful not to show in tables or figures symmetric error bars that would yield results that are out of range (e.g. negative error rates).
- If error bars are reported in tables or plots, The authors should explain in the text how they were calculated and reference the corresponding figures or tables in the text.

8. Experiments compute resources

Question: For each experiment, does the paper provide sufficient information on the computer resources (type of compute workers, memory, time of execution) needed to reproduce the experiments?

Answer: [\[Yes\]](#)

Justification: We report the compute resources used in Appendix J, including GPU usage and approximate training times for each dataset.

Guidelines:

- The answer NA means that the paper does not include experiments.
- The paper should indicate the type of compute workers CPU or GPU, internal cluster, or cloud provider, including relevant memory and storage.
- The paper should provide the amount of compute required for each of the individual experimental runs as well as estimate the total compute.
- The paper should disclose whether the full research project required more compute than the experiments reported in the paper (e.g., preliminary or failed experiments that didn't make it into the paper).

9. Code of ethics

Question: Does the research conducted in the paper conform, in every respect, with the NeurIPS Code of Ethics <https://neurips.cc/public/EthicsGuidelines>?

Answer: [Yes]

Justification: The research conform with the NeurIPS Code of Ethics.

Guidelines:

- The answer NA means that the authors have not reviewed the NeurIPS Code of Ethics.
- If the authors answer No, they should explain the special circumstances that require a deviation from the Code of Ethics.
- The authors should make sure to preserve anonymity (e.g., if there is a special consideration due to laws or regulations in their jurisdiction).

10. Broader impacts

Question: Does the paper discuss both potential positive societal impacts and negative societal impacts of the work performed?

Answer: [Yes]

Justification: The introduction highlights the importance of anomaly detection in industrial IoT systems, emphasizing its potential to improve system reliability and prevent failures.

Guidelines:

- The answer NA means that there is no societal impact of the work performed.
- If the authors answer NA or No, they should explain why their work has no societal impact or why the paper does not address societal impact.
- Examples of negative societal impacts include potential malicious or unintended uses (e.g., disinformation, generating fake profiles, surveillance), fairness considerations (e.g., deployment of technologies that could make decisions that unfairly impact specific groups), privacy considerations, and security considerations.
- The conference expects that many papers will be foundational research and not tied to particular applications, let alone deployments. However, if there is a direct path to any negative applications, the authors should point it out. For example, it is legitimate to point out that an improvement in the quality of generative models could be used to generate deepfakes for disinformation. On the other hand, it is not needed to point out that a generic algorithm for optimizing neural networks could enable people to train models that generate Deepfakes faster.
- The authors should consider possible harms that could arise when the technology is being used as intended and functioning correctly, harms that could arise when the technology is being used as intended but gives incorrect results, and harms following from (intentional or unintentional) misuse of the technology.
- If there are negative societal impacts, the authors could also discuss possible mitigation strategies (e.g., gated release of models, providing defenses in addition to attacks, mechanisms for monitoring misuse, mechanisms to monitor how a system learns from feedback over time, improving the efficiency and accessibility of ML).

11. Safeguards

Question: Does the paper describe safeguards that have been put in place for responsible release of data or models that have a high risk for misuse (e.g., pretrained language models, image generators, or scraped datasets)?

Answer: [NA]

Justification: The paper does not involve high-risk models or sensitive datasets.

Guidelines:

- The answer NA means that the paper poses no such risks.
- Released models that have a high risk for misuse or dual-use should be released with necessary safeguards to allow for controlled use of the model, for example by requiring that users adhere to usage guidelines or restrictions to access the model or implementing safety filters.

- Datasets that have been scraped from the Internet could pose safety risks. The authors should describe how they avoided releasing unsafe images.
- We recognize that providing effective safeguards is challenging, and many papers do not require this, but we encourage authors to take this into account and make a best faith effort.

12. Licenses for existing assets

Question: Are the creators or original owners of assets (e.g., code, data, models), used in the paper, properly credited and are the license and terms of use explicitly mentioned and properly respected?

Answer: [Yes]

Justification: We use publicly available datasets such as MSL, SWAT, WADI, and PSM, all of which are appropriately cited in the paper. The licenses of these datasets permit academic use. Any baseline code used for comparison is also cited, and usage complies with the corresponding open-source licenses. (see Appendices B for details).

Guidelines:

- The answer NA means that the paper does not use existing assets.
- The authors should cite the original paper that produced the code package or dataset.
- The authors should state which version of the asset is used and, if possible, include a URL.
- The name of the license (e.g., CC-BY 4.0) should be included for each asset.
- For scraped data from a particular source (e.g., website), the copyright and terms of service of that source should be provided.
- If assets are released, the license, copyright information, and terms of use in the package should be provided. For popular datasets, paperswithcode.com/datasets has curated licenses for some datasets. Their licensing guide can help determine the license of a dataset.
- For existing datasets that are re-packaged, both the original license and the license of the derived asset (if it has changed) should be provided.
- If this information is not available online, the authors are encouraged to reach out to the asset's creators.

13. New assets

Question: Are new assets introduced in the paper well documented and is the documentation provided alongside the assets?

Answer: [NA]

Justification: This work does not release new assets.

Guidelines:

- The answer NA means that the paper does not release new assets.
- Researchers should communicate the details of the dataset/code/model as part of their submissions via structured templates. This includes details about training, license, limitations, etc.
- The paper should discuss whether and how consent was obtained from people whose asset is used.
- At submission time, remember to anonymize your assets (if applicable). You can either create an anonymized URL or include an anonymized zip file.

14. Crowdsourcing and research with human subjects

Question: For crowdsourcing experiments and research with human subjects, does the paper include the full text of instructions given to participants and screenshots, if applicable, as well as details about compensation (if any)?

Answer: [NA]

Justification: This work does not involve any crowdsourcing or experiments with human subjects.

Guidelines:

- The answer NA means that the paper does not involve crowdsourcing nor research with human subjects.
- Including this information in the supplemental material is fine, but if the main contribution of the paper involves human subjects, then as much detail as possible should be included in the main paper.
- According to the NeurIPS Code of Ethics, workers involved in data collection, curation, or other labor should be paid at least the minimum wage in the country of the data collector.

15. Institutional review board (IRB) approvals or equivalent for research with human subjects

Question: Does the paper describe potential risks incurred by study participants, whether such risks were disclosed to the subjects, and whether Institutional Review Board (IRB) approvals (or an equivalent approval/review based on the requirements of your country or institution) were obtained?

Answer: [NA]

Justification: This work does not involve research with human subjects and therefore does not require IRB approval.

Guidelines:

- The answer NA means that the paper does not involve crowdsourcing nor research with human subjects.
- Depending on the country in which research is conducted, IRB approval (or equivalent) may be required for any human subjects research. If you obtained IRB approval, you should clearly state this in the paper.
- We recognize that the procedures for this may vary significantly between institutions and locations, and we expect authors to adhere to the NeurIPS Code of Ethics and the guidelines for their institution.
- For initial submissions, do not include any information that would break anonymity (if applicable), such as the institution conducting the review.

16. Declaration of LLM usage

Question: Does the paper describe the usage of LLMs if it is an important, original, or non-standard component of the core methods in this research? Note that if the LLM is used only for writing, editing, or formatting purposes and does not impact the core methodology, scientific rigorousness, or originality of the research, declaration is not required.

Answer: [NA]

Justification: The paper does not involve the use of large language models in any core methodological component; any such tools were only used for auxiliary writing or formatting, which does not require declaration.

Guidelines:

- The answer NA means that the core method development in this research does not involve LLMs as any important, original, or non-standard components.
- Please refer to our LLM policy (<https://neurips.cc/Conferences/2025/LLM>) for what should or should not be described.

A Proof of Theorems

Mutual Information and Representation Learning: In representation learning, we focus on how the representation Z extracted from the original data X retains information related to the target variable Y . Mutual information $I(Z; Y)$ measures the amount of information about Y contained in Z :

$$I(Z; Y) = \int_z \int_y p(z, y) \log \frac{p(z, y)}{p(z)p(y)} dy dz. \quad (11)$$

For discrete variables, the above integral becomes a summation. Equivalently,

$$I(Z; Y) = H(Y) - H(Y | Z). \quad (12)$$

Representation learning aims to balance information retention and representation complexity:

$$\mathcal{J}(Z) = I(Z; Y) - \lambda \mathcal{C}(Z), \quad (13)$$

where $\mathcal{C}(Z)$ measures complexity and $\lambda > 0$ controls the tradeoff. We consider a temporal encoder E_T and a topological encoder E_G :

$$Z_T = E_T(X), \quad Z_G = E_G(X), \quad Z = f(Z_T, Z_G | G). \quad (14)$$

Here $f(\cdot | G)$ is a graph-guided fusion mechanism. **Assumptions.** We assume the graph G is constructed from domain knowledge and is independent of both the target Y and the temporal representation Z_T :

$$I(G; Y) = 0, \quad I(G; Z_T) = 0. \quad (15)$$

Theorem 1 (Graph-Conditioned Information Bound)

Let $Z = f(Z_T, Z_G | G)$ be the fused representation. Then

$$I(Z; Y) \leq \min\{I(X; Y), I(Z_T, Z_G; Y | G)\}. \quad (16)$$

Moreover, under the above assumptions, one obtains

$$I(Z; Y) \leq I(Z_T; Y) + I(Z_G; Y | Z_T). \quad (17)$$

By the Data Processing Inequality (DPI) and the Markov chain $X \rightarrow (Z_T, Z_G, G) \rightarrow Z$, we have

$$I(Z; Y) \leq I(X; Y). \quad (18)$$

Similarly,

$$I(Z; Y) \leq I(Z_T, Z_G, G; Y). \quad (19)$$

Applying the chain rule to $I(Z_T, Z_G, G; Y)$ gives

$$I(Z_T, Z_G, G; Y) = I(G; Y) + I(Z_T, Z_G; Y | G). \quad (20)$$

Under (15), $I(G; Y) = 0$, hence

$$I(Z; Y) \leq I(Z_T, Z_G; Y | G). \quad (21)$$

Next, by chain rule decomposition,

$$I(Z_T, Z_G; Y | G) = I(Z_T; Y | G) + I(Z_G; Y | Z_T, G). \quad (22)$$

By the independence $I(G; Z_T) = 0$ and the fact that conditioning cannot increase mutual information,

$$I(Z_T; Y | G) = I(Z_T; Y), \quad I(Z_G; Y | Z_T, G) \leq I(Z_G; Y | Z_T). \quad (23)$$

Combining (21)–(23) yields (17). Finally, merging with (18) gives the bound in (16).

Remark. The contrastive loss in our model maximizes a lower bound on $I(Z_T; Z_G | G)$, encouraging complementary information extraction under graph constraints.

Theorem 2 (Graph-Conditioned Mutual Information Maximization with Asymmetric Encoders)

Let $Z_T = p_\theta(E_T(X))$ and $Z_G = \text{sg}(E_G(X))$ be the temporal and topological representations under graph G , where p_θ is a predictor and $\text{sg}(\cdot)$ denotes stop-gradient. The contrastive loss:

$$\mathcal{L}_{\text{contrast}} = -\mathbb{E}_{\substack{(s,d) \sim G \\ \mathcal{B}}} \left[\log \frac{\exp(s_\theta(Z_T[s], Z_G[d]))}{\sum_{d' \in \mathcal{B}} \exp(s_\theta(Z_T[s], Z_G[d']))} \right]. \quad (24)$$

achieves:

$$I(Z_T; Z_G | G) \geq \log(|\mathcal{B}| - 1) - \mathcal{L}_{\text{contrast}}. \quad (25)$$

Proof: The proof builds on the variational lower bound for mutual information and its connection to contrastive learning. Variational Lower Bound of Conditional MI. Following the variational framework for mutual information estimation [Oord et al., 2018, Poole et al., 2019], then define conditional mutual information:

$$I(Z_T; Z_G | G) = \mathbb{E}_{(s,d) \sim G} \left[\mathbb{E}_{Z_T[s], Z_G[d]} \log \frac{p(Z_T[s]; Z_G[d] | G)}{p(Z_T[s] | G) p(Z_G[d] | G)} \right]. \quad (26)$$

Introduce variational distribution $q(Z_G[d] | Z_T[s], G)$ to approximate the true conditional distribution. According to the variational lower bound, we get:

$$I(Z_T; Z_G | G) \geq \mathbb{E}_{(s,d) \sim G} \left[\mathbb{E}_{Z_T[s], Z_G[d]} \log \frac{q(Z_G[d] | Z_T[s], G)}{p(Z_G[d] | G)} \right]. \quad (27)$$

Then, maximize the lower bound by contrast loss:

Assume the scoring function is normalized cosine similarity:

$$s_\theta(Z_T[s], Z_G[d]) = \frac{\langle p_\theta(Z_T[s]), Z_G[d] \rangle}{\tau \|p_\theta(Z_T[s])\| \|Z_G[d]\|}. \quad (28)$$

Define variational distribution:

$$q(Z_G[d] | Z_T[s], G) = \frac{\exp(s_\theta(Z_T[s], Z_G[d]))}{\sum_{d' \in \mathcal{B}} \exp(s_\theta(Z_T[s], Z_G[d']))}. \quad (29)$$

Substituting into the variational lower bound we get:

$$I(Z_T; Z_G | G) \geq \mathbb{E}_{(s,d) \sim G} \left[s_\theta(Z_T[s], Z_G[d]) - \log \sum_{d' \in \mathcal{B}} \exp(s_\theta(Z_T[s], Z_G[d'])) \right]. \quad (30)$$

Contrast loss $\mathcal{L}_{\text{contrast}}$ It can be rewritten as:

$$\mathcal{L}_{\text{contrast}} = -\mathbb{E}_{(s,d) \sim G} [s_\theta(Z_T[s], Z_G[d])] + \mathbb{E}_s \left[\log \sum_{d' \in \mathcal{B}} \exp(s_\theta(Z_T[s], Z_G[d'])) \right]. \quad (31)$$

Combining the two equations, we can get the final lower bound:

$$I(Z_T; Z_G | G) \geq \log(|\mathcal{B}| - 1) - \mathcal{L}_{\text{contrast}}. \quad (32)$$

Therefore, Minimizing the contrastive loss $\mathcal{L}_{\text{contrast}}$ is equivalent to maximizing a lower bound on the conditional mutual information $I(Z_T; Z_G | G)$, and this optimization inherently encourages the temporal embedding Z_T and the topological embedding Z_G to share as much graph-constrained information as possible.

B Experimental details

B.1 Datasets

Our model ScatterAD is evaluated on six real world multivariate datasets. The specific descriptions of the datasets are shown in the following table.

Table 3: Dataset statistics used in our experiments. “Dims” denotes the number of dimensions (variables). “Train” and “Test” indicate the number of time points in training and labeled test sets, respectively. “AR” denotes the anomaly rate (%).

Benchmark	Source	Dims	Train	Test (labeled)	AR (%)
MSL	NASA Space Sensors	55	58,317	73,729	10.48
PSM	eBay Server Machine	25	132,481	87,941	27.76
SWaT	Infrastructure System	51	495,000	449,919	12.14
WADI	Infrastructure System	123	1,209,601	172,801	5.71
NIPS-TS-GECCO	Water Quality for IoT	9	69,260	69,260	1.10
NIPS-TS-SWAN	Solar Weather (Space)	38	60,000	60,000	32.60

The SWaT and WADI datasets can be obtained by filling out the following form: https://docs.google.com/forms/d/1GOLYXa7TX0KlayqugU00PMvbewSQiGNM0jHuNqKcieA/viewform?edit_requested=true

B.2 Baselines

For all baseline comparisons, we rely on their official codebases and adopt the hyperparameter settings as suggested in the respective publications. The corresponding source codes are publicly accessible at the URLs provided below.

Sub-Trans (IJCAI’24) https://github.com/jackyue1994/sub_adjacent_transformer
ModernTCN (ICLR’24) <https://github.com/luodhhh/ModernTCN>
iTransformer (ICLR’24) <https://github.com/thuml/iTransformer>
TopoGDN (CIKM’24) <https://github.com/ljj-cyber/topogdn>
DCdetector (KDD’23) <https://github.com/DAMO-DI-ML/KDD2023-DCdetector>
MEMTO (NeurIPS’23) <https://github.com/gunny97/MEMTO>
DuoGAT (CIKM’23) <https://github.com/ByeongtaePark/DuoGAT>
MTGFlow (AAAI’23) <https://github.com/zqhang/MTGFLW>
GANF (ICLR’22) <https://github.com/EnyanDai/GANF>
AnomalyTrans (ICLR’22) <https://github.com/thuml/Anomaly-Transformer>
VAE <https://github.com/yzhao062/pyod/blob/master/pyod/models/vae.py>
IF <https://github.com/yzhao062/pyod/blob/master/pyod/models/iforest.py>
PCA <https://github.com/yzhao062/pyod/blob/master/pyod/models/pca.py>

B.3 Evaluation Metrics

In anomaly detection evaluation, to comprehensively assess model performance across diverse anomaly detection scenarios, we adopt a unified evaluation protocol inspired by Liu et al. [Liu and Paparrizos, 2024], covering both label-based and score-based metrics.

For label-based evaluation We use the Affiliated-Precision (Aff-P), Affiliated-Recall (Aff-R), and Affiliated-F1 (Aff-F) [Huet et al., 2022], which aim to better reflect the proximity between predicted and true anomaly ranges. For completeness, we also include the widely used yet imperfect point-adjusted metric, including Point-Adjusted-Precision (PA-P), Point-Adjusted-Recall (PA-R) and Point-Adjusted-F1 (PA-F).

score-based evaluation We employ conventional metrics such as (AUC-PR) and (AUC-ROC), along with their range-based extensions, Range-AUC-PR (R-A-P) and Range-AUC-ROC (R-A-R) [Paparrizos et al., 2022], which consider anomaly duration and sequential nature to more comprehensively reflect model performance. Additionally, we incorporate the Volume Under the Surface measures, VUS-ROC(V-ROC) and VUS-PR(V-PR) [Paparrizos et al., 2022], which enhance anomaly score reliability and interpretability by introducing tolerance buffers around anomaly boundaries and using continuous labels.

B.4 Implementation Details

All experiments were performed in Python 3.9 using PyTorch and on NVIDIA Tesla-A800 GPUs. We used the Adam optimizer during training. Initially, the batch size was set to 128, and the time window size was uniformly set to 110 for all datasets except NIPS-TS-GECCO(N-T-W) and NIP-TS-Swan(N-T-S), which were set to 90. The GAT in ScatterAD has H=4 attention heads per layer and a hidden dimension of 512. For hyperparameter tuning, the training set was temporarily divided into 80% for training and 20% for validation. For each dataset, the learning rate was uniformly set to 0.0001.

C Additional Experiments

Due to space constraints in the main text, we present additional experimental results in this section. In particular, we further evaluate the performance using the following metrics: Range-AUC-ROC and Range-AUC-PR, VUS-ROC and VUS-PR, Affiliated Precision, Affiliated Recall and Affiliated F1, as well as point-adjusted metrics including PA-P, PA-R and PA-F. The reported results are averaged over multiple runs to ensure reliability.

Table 4: Quantitative comparison of four evaluation metrics. R-A-R and R-A-P are Range-AUC-ROC and Range-AUC-PR. V-ROC and V-PR are volumes under the surfaces created based on the ROC curve and PR curve. **Bold** indicates the optimal performance; Underline indicates the suboptimal performance.

Dataset	Metric	Ours	S.T.	T.G.	Memto	DC.	M.TCN	iT.	MTG	A.T.	D.G.	GANF	VAE	IF	PCA
MSL	R-A-R	0.920	0.750	0.695	0.704	<u>0.913</u>	0.756	0.655	0.748	0.891	0.613	0.846	0.725	0.641	0.633
	R-A-P	0.919	0.754	0.826	0.643	<u>0.891</u>	0.745	0.638	0.753	0.875	0.574	0.733	0.630	0.654	0.651
	V-ROC	0.872	0.745	0.705	0.601	0.904	0.748	0.647	0.648	<u>0.884</u>	0.512	0.644	0.626	0.743	0.641
	V-PR	0.885	0.752	0.785	0.639	<u>0.883</u>	0.737	0.631	0.727	0.864	0.573	0.678	0.631	0.656	0.652
PSM	R-A-R	0.889	0.731	0.764	0.820	0.911	0.781	0.738	0.703	0.874	0.588	0.686	0.641	0.692	0.616
	R-A-P	0.918	0.806	0.591	0.871	0.925	0.841	0.808	0.831	0.865	0.629	0.821	0.571	0.712	0.671
	V-ROC	0.879	0.729	0.641	0.814	<u>0.861</u>	0.784	0.741	0.707	0.844	0.583	0.687	0.574	0.652	0.516
	V-PR	0.911	0.798	0.795	0.867	0.888	0.842	0.808	0.825	<u>0.904</u>	0.525	0.813	0.738	0.659	0.569
SWaT	R-A-R	0.942	0.956	0.734	0.710	0.967	0.791	0.931	0.539	<u>0.952</u>	0.563	0.568	0.732	0.638	0.663
	R-A-P	0.915	0.868	0.646	0.678	0.941	0.772	0.886	0.551	0.795	0.484	0.424	0.648	0.674	0.694
	V-ROC	0.945	0.938	0.776	0.713	0.970	0.791	0.924	0.540	<u>0.954</u>	0.322	0.563	0.842	0.548	0.707
	V-PR	0.917	0.870	0.637	0.681	0.944	0.771	0.881	0.551	0.796	0.383	0.414	0.656	0.678	0.689
WADI	R-A-R	0.927	0.945	0.623	0.866	0.912	0.561	0.629	0.614	0.955	0.413	0.617	0.692	0.714	0.677
	R-A-P	0.846	<u>0.843</u>	0.588	0.797	0.773	0.265	0.359	0.637	0.794	0.442	0.639	0.549	0.434	0.547
	V-ROC	0.877	0.943	0.627	0.758	0.937	0.573	0.631	0.618	0.956	0.412	0.620	0.692	0.719	0.669
	V-PR	0.799	0.854	0.576	0.659	0.786	0.276	0.359	0.634	0.796	0.441	0.634	0.549	0.439	0.542
NIPS-TS-SWAN	R-A-R	0.858	0.870	0.607	0.882	0.881	0.872	0.866	0.843	<u>0.878</u>	0.729	0.748	0.807	0.702	0.794
	R-A-P	0.941	0.936	0.587	0.851	0.948	0.946	0.944	0.879	0.929	0.705	0.781	0.639	0.646	0.743
	V-ROC	0.829	0.851	0.607	0.873	0.861	0.853	0.847	0.805	<u>0.866</u>	0.607	0.807	0.755	0.691	0.681
	V-PR	0.932	0.925	0.587	0.929	0.935	0.933	0.931	0.858	0.918	0.687	0.759	0.629	0.637	0.633
NIPS-TS-GECCO	R-A-R	0.721	0.536	0.599	0.523	0.629	0.522	0.523	0.566	0.581	0.522	0.564	0.614	<u>0.635</u>	0.626
	R-A-P	0.587	0.318	<u>0.585</u>	0.483	0.345	0.311	0.367	0.566	0.349	0.519	0.526	0.561	0.522	0.517
	V-ROC	0.748	0.541	0.589	0.527	0.623	0.521	0.521	0.568	0.576	0.513	0.565	<u>0.669</u>	0.665	0.624
	V-PR	0.611	0.323	0.582	0.479	0.339	0.314	0.353	0.546	0.443	0.512	0.505	<u>0.597</u>	0.582	0.554
#1 Count		12	1	0	2	9	0	0	0	2	0	0	0	0	0

Table 5: Performance comparison across six benchmark datasets using affinity-based precision (Aff-P), recall (Aff-R), and F1 score (Aff-F). Our method consistently outperforms others, especially in Aff-F. **Bold** indicates the optimal performance; Underline indicates the suboptimal performance.

Dataset	Metric	Ours	S.T.	T.G.	Memto	DC.	M.TCN	iT.	MTG	A.T.	D.G.	GANF	VAE	IF	PCA
MSL	Aff-P	0.994	0.549	0.709	0.515	0.516	0.588	0.559	<u>0.921</u>	0.518	0.512	0.762	0.587	0.423	0.694
	Aff-R	0.782	0.871	0.642	0.704	<u>0.972</u>	0.893	0.785	0.234	0.961	0.998	0.205	0.714	0.342	0.512
	Aff-F	0.867	0.673	0.674	0.595	0.674	<u>0.709</u>	0.652	0.374	0.673	0.677	0.323	0.642	0.374	0.591
PSM	Aff-P	0.746	0.774	0.627	0.641	0.561	0.664	0.644	0.967	0.551	0.465	<u>0.961</u>	0.755	0.469	0.389
	Aff-R	0.846	0.798	0.764	0.677	0.783	0.743	0.662	0.282	0.814	0.945	0.198	0.412	0.731	0.312
	Aff-F	0.797	<u>0.786</u>	0.689	0.659	0.653	0.701	0.652	0.436	0.657	0.624	0.329	0.524	0.569	0.437
SWaT	Aff-P	0.567	0.582	0.538	0.554	0.531	0.586	0.581	<u>0.662</u>	0.571	0.478	0.552	0.499	0.743	0.387
	Aff-R	0.926	0.689	0.663	0.635	0.981	0.827	0.934	0.356	0.683	0.878	0.676	0.642	0.363	0.725
	Aff-F	0.704	0.631	0.594	0.592	0.687	0.685	0.716	0.463	0.622	0.619	0.608	0.563	0.502	0.537
WADI	Aff-P	0.714	0.632	0.652	0.545	0.619	0.546	0.573	0.771	0.553	0.476	<u>0.751</u>	0.456	0.658	0.601
	Aff-R	0.525	0.956	0.449	<u>0.981</u>	0.874	0.571	0.809	0.598	0.985	0.957	0.601	0.726	0.482	0.365
	Aff-F	0.605	0.756	0.532	0.701	<u>0.725</u>	0.558	0.671	0.673	0.708	0.636	0.667	0.556	0.555	0.477
NIPS-TS-SWAN	Aff-P	0.754	0.798	0.521	0.525	0.531	0.515	0.491	0.998	0.672	0.509	0.435	0.374	0.711	0.645
	Aff-R	0.019	0.824	0.997	0.017	0.445	0.554	0.526	0.002	0.054	<u>0.935</u>	0.003	0.396	0.318	0.731
	Aff-F	0.038	0.805	<u>0.685</u>	0.033	0.484	0.533	0.507	0.003	0.099	0.659	0.005	0.385	0.438	0.680
NIPS-TS-GECCO	Aff-P	0.829	<u>0.805</u>	0.508	0.638	0.513	0.555	0.541	0.706	0.533	0.501	0.592	0.732	0.402	0.539
	Aff-R	0.820	0.337	0.702	0.317	<u>0.883</u>	0.373	0.365	0.231	0.859	0.998	0.173	0.362	0.698	0.481
	Aff-F	0.825	0.476	0.589	0.424	0.648	0.446	0.435	0.348	<u>0.658</u>	0.667	0.268	0.481	0.531	0.509
#1 Count		6	2	1	0	1	0	1	3	1	3	0	0	1	0

Table 6: Performance comparison in terms of PA-Precision (PA-P), PA-Recall (PA-R), and PA-F1 (PA-F) on six benchmark datasets. **Bold** indicates the optimal performance; Underline indicates the suboptimal performance.

Dataset	Metric	Ours	S.T.	T.G.	Memto	DC.	M.TCN	iT.	MTG	A.T.	D.G.	GANF	VAE	IF	PCA
MSL	PA-P	0.933	0.931	0.626	0.971	0.922	0.884	0.825	0.744	<u>0.917</u>	0.742	0.422	0.421	0.509	0.472
	PA-R	0.997	0.803	0.836	0.504	<u>0.974</u>	0.743	0.548	0.574	0.951	0.582	0.584	0.635	0.723	0.416
	PA-F	0.964	0.863	0.714	0.664	<u>0.947</u>	0.807	0.659	0.648	0.934	0.652	0.489	0.512	0.598	0.444
PSM	PA-P	0.985	0.980	0.784	<u>0.989</u>	0.971	0.975	0.962	0.992	0.973	0.837	0.994	0.691	0.374	0.647
	PA-R	0.977	0.904	0.819	0.966	<u>0.984</u>	0.954	0.893	0.666	0.983	0.731	0.652	0.524	0.739	0.337
	PA-F	0.981	0.941	0.801	0.977	0.977	0.965	0.926	0.797	<u>0.978</u>	0.780	0.788	0.596	0.534	0.467
SWaT	PA-P	0.931	0.809	0.827	0.889	0.931	0.894	0.874	0.952	0.892	0.786	0.548	0.585	0.651	0.443
	PA-R	0.973	0.923	0.754	0.659	0.949	0.875	0.962	0.338	0.992	0.863	0.157	0.477	0.328	<u>0.721</u>
	PA-F	0.951	0.863	0.788	0.756	0.939	0.884	0.916	0.500	<u>0.943</u>	0.822	0.244	0.526	0.472	0.548
WADI	PA-P	0.813	0.856	0.841	0.751	0.607	0.291	0.355	0.875	0.637	<u>0.866</u>	0.847	0.658	0.372	0.547
	PA-R	0.917	0.890	0.829	0.874	<u>0.917</u>	0.372	0.511	0.570	0.947	0.595	0.570	0.416	0.612	0.723
	PA-F	0.862	0.873	0.834	0.807	0.731	0.326	0.419	0.690	0.738	0.705	0.681	0.512	0.474	0.618
NIPS-TS-SWAN	PA-P	<u>0.991</u>	0.997	0.694	0.988	0.966	0.954	0.952	0.662	0.972	0.591	0.695	0.633	0.364	0.699
	PA-R	0.585	0.556	<u>0.629</u>	0.526	0.591	0.592	0.591	0.533	0.540	0.438	0.576	0.395	0.738	0.403
	PA-F	0.736	<u>0.714</u>	0.660	0.687	0.733	0.731	0.729	0.591	0.695	0.503	0.630	0.497	0.522	0.526
NIPS-TS-GECCO	PA-P	0.669	0.524	0.582	0.889	0.391	0.404	0.471	0.371	0.277	0.539	0.346	0.382	<u>0.548</u>	0.466
	PA-R	0.944	0.463	<u>0.789</u>	0.352	0.597	0.321	0.321	0.391	0.391	0.745	0.364	0.672	0.422	0.735
	PA-F	0.784	0.491	<u>0.670</u>	0.504	0.472	0.357	0.381	0.381	0.325	0.625	0.355	0.491	0.481	0.583
#1 Count		6	2	0	2	0	0	0	2	3	0	1	0	1	0

D Analysis on the Universality and Robustness of the Scattering Phenomenon

To investigate the universality of the scattering phenomenon and evaluate the model’s robustness, we conduct a quantitative analysis across all six benchmark datasets under varying levels of noise. Specifically, we inject additive Gaussian noise with four different intensities ($\sigma \in \{0, 0.5, 1.0, 2.0\}$) into the normalized test data, where $\sigma = 0.0$ serves as the no-noise baseline. We then quantify the model’s internal discriminative power by calculating the average scattering score for both normal and anomalous samples. This score is defined as the mean Euclidean distance of samples to their respective class center. The separation ratio between these scores (Anomalous/Normal) is analyzed to measure class distinguishability, with results presented in Table 7.

Table 7: Analysis of scattering scores and their separation ratio under different Gaussian noise levels (σ). A separation ratio greater than 1.0 suggests that anomalous samples are, on average, farther from their class center than the normal samples, confirming the scattering phenomenon.

Dataset	Noise Level (σ)	Scattering Score (Normal)	Scattering Score (Anomalous)	Separation Ratio(%)
MSL	0.0	16.0	18.2	1.14
	0.5	21.6	31.6	1.46
	1.0	36.0	49.3	1.37
	2.0	65.9	84.6	1.28
PSM	0.0	31.5	37.8	1.20
	0.5	33.1	40.3	1.22
	1.0	41.2	47.4	1.15
	2.0	61.1	65.7	1.08
SWaT	0.0	73.10	94.09	1.29
	0.5	75.63	95.71	1.27
	1.0	79.22	98.03	1.24
	2.0	84.50	102.11	1.21
WADI	0.0	0.78	1.16	1.49
	0.5	34.9	43.4	1.24
	1.0	87.1	72.4	0.83
	2.0	166.7	137.0	0.82
NIPS-TS-SWAN	0.0	20.2	28.4	1.41
	0.5	21.8	32.4	1.49
	1.0	27.7	42.2	1.52
	2.0	42.1	65.5	1.56
NIPS-TS-GECCO	0.0	21.60	95.97	4.44
	0.5	26.10	105.33	4.04
	1.0	40.70	41.40	1.02
	2.0	68.60	197.30	2.88

The results presented in Table 7 clearly reveal a consistent anomaly scattering pattern across the six diverse, real-world datasets. Notably, for the WADI dataset, the scattering score of normal samples surpasses that of anomalies under medium-to-high noise conditions ($\sigma \geq 1.0$), resulting in a separation ratio less than 1.0. We attribute this phenomenon to WADI’s high dimensionality (123 dimensions), where strong noise may have a compounding effect and lead to complex changes in inter-variable correlations. This finding indicates that while our method is generally robust across various noisy environments, its performance may be sensitive to strong noise when applied to extremely high-dimensional datasets that feature subtle anomaly patterns. This analysis helps to comprehensively characterize the performance boundaries of our method.

E Parameter Sensitivity Analysis

We analyze the sensitivity of ScatterAD to key hyperparameters across six datasets (Figure 7). The model performs consistently across varying window sizes, demonstrating robustness to both short- and long-range temporal contexts. A window size of 110 yields the highest AUC-ROC and is thus

used in all experiments. Therefore, this brief window size is selected in our experiments. We further studied the sensitivity of the other 2 parameters: the dimension of the hidden layer and the number of encoder layers. For encoder depth, two layers consistently achieve the best performance while keeping the model lightweight. Increasing the hidden dimension improves performance, and we choose 512 as a balanced default to maintain model efficiency.

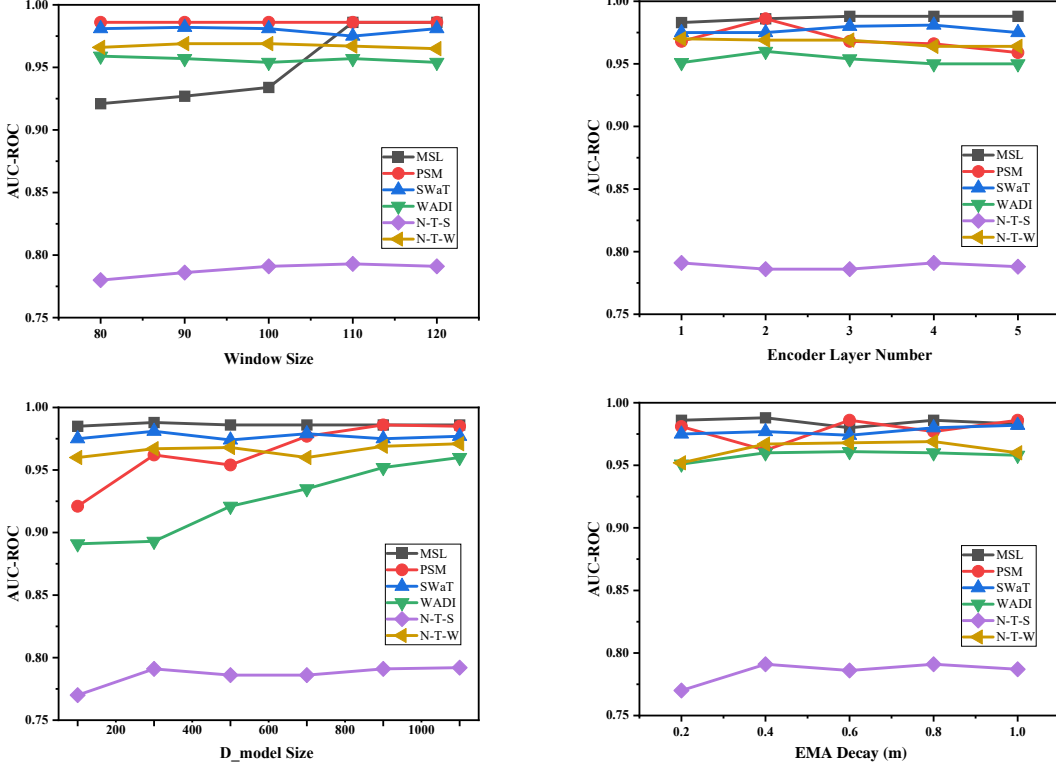


Figure 7: Parameter sensitivity analysis in ScatterAD.

Anomaly threshold σ is a important hyperparameter, which may affect the determination of anomaly or not. We have a default value of 1 for all benchmarks. As shown in Table8, when it is in the range of 0.5 to 1, it has little effect on the final model performance. PSM and SMAP are also more robust to anomaly thresholds than MSL. For the three benchmarks, its best results appear when σ equals 0.8 or 1.

Table 8: Sensitivity analysis of the hyperparameter δ on six datasets. Metrics: AF (Affiliated-F1), AR (AUC-ROC). Best values per column are highlighted in bold.

Dataset	MSL		PSM		SWaT		WADI		N-T-S		N-T-W	
Metric	AF	AR										
$\delta = 0.2$	0.863	0.986	0.789	0.955	0.656	0.517	0.929	0.944	0.029	0.786	0.799	0.954
$\delta = 0.4$	0.861	0.982	0.793	0.952	0.698	0.521	0.934	0.974	0.038	0.792	0.803	0.964
$\delta = 0.6$	0.843	0.978	0.783	0.946	0.704	0.586	0.961	0.975	0.035	0.790	0.814	0.965
$\delta = 0.8$	0.855	0.981	0.794	0.969	0.701	0.587	0.960	0.957	0.038	0.792	0.818	0.959
$\delta = 1.0$	0.867	0.986	0.792	0.969	0.702	0.583	0.955	0.957	0.037	0.789	0.823	0.969

F Analysis of Performance on the NIPS-TS-SWAN Dataset

A notable performance discrepancy is observed on the NIPS-TS-SWAN dataset, specifically concerning the Affiliated-F1 (Aff-F1) metric. It is important to first establish that our proposed model, ScatterAD, successfully generates separable anomaly scores for this dataset. The high Point-Adjusted F1 (PA-F1) score of 0.736 (as reported in Table 1) demonstrates that anomalous events are correctly assigned higher scores than normal ones at the point level.

To investigate the low Aff-F1 score, we hypothesize that the metric itself may be overly sensitive to minor localization errors on this particular dataset. To test this, we devised a controlled simulation experiment, independent of our model, to evaluate the intrinsic robustness of the Aff-F1 metric. In this simulation, we assume a perfect model whose predictions exactly match the ground truth (achieving an F1 score of 1.0). We then introduce a minor, realistic localization error by shifting the entire prediction sequence by a small number of timesteps (Δt) and observe the resulting changes in both Aff-F1 and a traditional point-wise F1 score. The experiment is also conducted on the MSL dataset for comparison.

Table 9: Sensitivity analysis of F1 metrics to temporal localization errors. A perfect prediction sequence is shifted by a few timesteps, and the degradation of segment-level (Aff-F1) and point-level F1 scores is measured.

Dataset	Localization Error (Shift in steps)	Aff-F1 Score (Segment-level)	Point-wise F1 (Point-level)
NIPS-TS-SWAN	0 steps	1.000	1.000
	1 step	0.065 (93.5%↓)	0.686
	2 steps	0.174	0.697
	5 steps	0.223	0.704
	10 steps	0.226	0.709
MSL	0 steps	1.000	1.000
	1 step	1.000	0.995
	2 steps	1.000	0.991
	5 steps	0.972 (2.8%↓)	0.977
	10 steps	0.889	0.954

The results in Table 9 are revealing. For the NIPS-TS-SWAN dataset, a minuscule localization shift of just one timestep causes the Aff-F1 score to plummet from 1.0 to 0.065, a 93.5% reduction. In stark contrast, the same shift on the MSL dataset has no impact on the Aff-F1 score, and even a 5-step shift results in only a minor 2.8% drop. This demonstrates the extreme sensitivity of the Aff-F1 metric specifically on the NIPS-TS-SWAN dataset. This inherent characteristic of the metric and dataset interaction explains why our model, along with many other state-of-the-art methods (as shown in Table 1), exhibits poor performance on this particular metric. Conversely, the more traditional point-wise F1 score shows much greater resilience. This justifies our decision to report both scores for a balanced and comprehensive evaluation.

To further validate our model’s detection capability at a macro level, we compiled overall prediction statistics for ScatterAD on the NIPS-TS-SWAN dataset, shown in Table 10.

Table 10: Macro-level prediction statistics for ScatterAD on the NIPS-TS-SWAN dataset.

Statistic	Ground Truth	Our Prediction
Total Anomaly Ratio	32.6%	32.1%
Number of Anomaly Segments	551,937	843,596

The statistics show that the total proportion of anomalies predicted by ScatterAD (32.1%) closely aligns with the ground truth (32.6%), demonstrating its accurate high-level detection capability. However, the model identifies a higher number of individual anomaly segments. This suggests that the

model may tend to partition a single continuous ground-truth anomaly into several smaller, consecutive segments. Consequently, due to such minor, unavoidable localization offsets, its performance is significantly underestimated by the strict segment-matching criteria of the Aff-F1 metric under these specific data conditions.

G Analysis of the Scattering Center Initialization

The initialization strategy for the scattering center, \mathbf{c} , is a key design consideration impacting model stability and the potential for learning suboptimal solutions. In our framework, the scattering center \mathbf{c} is initialized once at the beginning of each training run and remains fixed throughout the training process; it is not a learnable parameter updated via backpropagation. The role of this fixed center is twofold:

- **Provide a Fixed Anchor Point:** The center \mathbf{c} offers a stable, convergent target direction for the representations of normal samples. This guides the model to learn a mapping that projects these representations into a compact region on the latent hypersphere.
- **Break Symmetry and Regularize:** A fixed, predefined center (e.g., a canonical basis vector like $[1, 0, \dots, 0]$) might introduce an undesirable bias, potentially inducing the model to learn a trivial solution where all normal samples map to a specific axis. By randomly initializing \mathbf{c} , we avoid this risk and compel the model to learn more generalizable, rotation-invariant representations. This can be viewed as a form of implicit stochastic regularization, preventing the model from overfitting to a predefined direction in the latent space.

G.1 Stability Analysis

To empirically validate the stability of this random initialization strategy, we conducted an experiment by repeating the full training and evaluation process with 5 different random seeds on the MSL and PSM datasets. A different seed results in a different initialization for the scattering center \mathbf{c} . As shown in Table 11, the standard deviation of the performance metrics is extremely low, confirming that the model’s performance is robust and not sensitive to the specific random choice of the center.

Table 11: Stability analysis of the random scattering center initialization across 5 runs with different random seeds. The low standard deviation indicates high stability.

Dataset	Metric	Original	Mean	Std. Dev.
MSL	Aff-F1	0.865	0.865	± 0.003
	A-ROC	0.986	0.986	± 0.001
PSM	Aff-F1	0.797	0.797	± 0.002
	A-ROC	0.986	0.986	± 0.003

G.2 Ablation Study on Initialization Strategies

Furthermore, to demonstrate the effectiveness of our chosen approach, we performed an ablation study comparing several alternative center initialization strategies:

- **Zero:** Initialize the center at the origin (zero vector) to test the simplest symmetric starting point.
- **Fixed-Radius:** Initialize the center on a hypersphere with a fixed radius to test the model’s sensitivity to the initial magnitude.
- **Multi-center:** Use multiple independent scattering centers to test the model’s ability to capture potentially multi-modal distributions of normal data.

The results, presented in Table 12, compare these strategies with the `random_in_ball` approach (randomly selecting a point within the unit hypersphere) proposed in our paper. The findings confirm

that our model is not sensitive to the specific initialization strategy of \mathbf{c} . The performance remains consistently high across different methods, indicating that the `random_in_ball` strategy is a simple, robust, and effective choice that avoids the need for additional hyperparameter tuning (e.g., setting a radius or the number of centers).

Table 12: Ablation study of different scattering center initialization strategies. Performance metrics (Aff-F1 and AUC ROC) remain stable across various strategies, validating the robustness of our approach.

Dataset	Center Strategy	Num Centers	Radius	Aff-F1	AUC-ROC
MSL	<code>random_in_ball</code> (Ours)	1	N/A	0.867	0.986
	<code>zero</code>	1	0.0	0.866	0.986
	<code>fixed_radius</code>	1	0.3	0.866	0.986
	<code>fixed_radius</code>	1	0.7	0.864	0.986
	<code>multi-center</code>	3	N/A	0.869	0.986
PSM	<code>random_in_ball</code> (Ours)	1	N/A	0.797	0.986
	<code>zero</code>	1	0.0	0.797	0.986
	<code>fixed_radius</code>	1	0.3	0.797	0.986
	<code>fixed_radius</code>	1	0.7	0.796	0.986
	<code>multi-center</code>	3	N/A	0.792	0.980
SWaT	<code>random_in_ball</code> (Ours)	1	N/A	0.704	0.982
	<code>zero</code>	1	0.0	0.704	0.982
	<code>fixed_radius</code>	1	0.3	0.698	0.977
	<code>fixed_radius</code>	1	0.7	0.702	0.979
	<code>multi-center</code>	3	N/A	0.702	0.980

H Robustness to Graph Topology

To evaluate the model’s sensitivity and robustness to the graph structure, we conducted an experiment to simulate dynamically changing graph topologies. We extended our data loading process to generate a different graph structure for each input time window during both training and inference. This contrasts with our main approach of using a single, static graph learned from the training data. We designed two dynamic topology generation strategies:

- **Random Topology:** For each time window, connections between nodes are randomly established with a fixed probability (`edge_prob=0.3`). To ensure basic graph connectivity, the connections between physically adjacent nodes are always preserved. This strategy simulates scenarios where inter-sensor correlations are irregular and appear randomly over time.
- **K-Nearest Neighbors (KNN) Topology:** For each time window, a topology is constructed by computing the Euclidean distance between the time series of each node and all other nodes within that window. Each node is then connected to its k -nearest neighbors (we use $k = 3$).

The performance and efficiency of these dynamic strategies were compared against our original static graph approach on the MSL and PSM datasets. The results are presented in Table 13.

The results in Table 13 indicate that the model’s detection performance is highly robust to the underlying graph structure. While dynamic topology strategies lead to marginal performance improvements in some specific cases (e.g., Random Topology on MSL and KNN Topology on PSM), the overall accuracy metrics remain remarkably stable across all three approaches. However, these dynamic strategies introduce significant computational overhead, as evidenced by the substantially lower throughput and higher average inference times. This analysis demonstrates that our proposed model

Table 13: Performance and efficiency comparison between static (Original) and dynamic graph topology strategies. While dynamic strategies offer marginal performance changes, they incur significant computational overhead, reducing throughput and increasing inference time.

Dataset	Strategy	Aff-F	PA-F	A-ROC	A-PR	Throughput (samples/sec)	Avg. Inference Time (ms)
MSL	Original (Ours)	0.866	0.964	0.986	0.932	60.35	16.57
	Random Topology	0.867	0.967	0.987	0.937	38.33	26.09
	KNN Topology	0.862	0.961	0.984	0.927	49.17	20.34
PSM	Original (Ours)	0.797	0.981	0.986	0.969	62.17	16.09
	Random Topology	0.791	0.975	0.980	0.961	31.77	31.47
	KNN Topology	0.803	0.966	0.971	0.948	25.66	38.98

exhibits strong robustness to graph topology, and employing a static graph derived from the training data strikes an excellent balance between detection effectiveness and computational efficiency.

I Convergence analysis

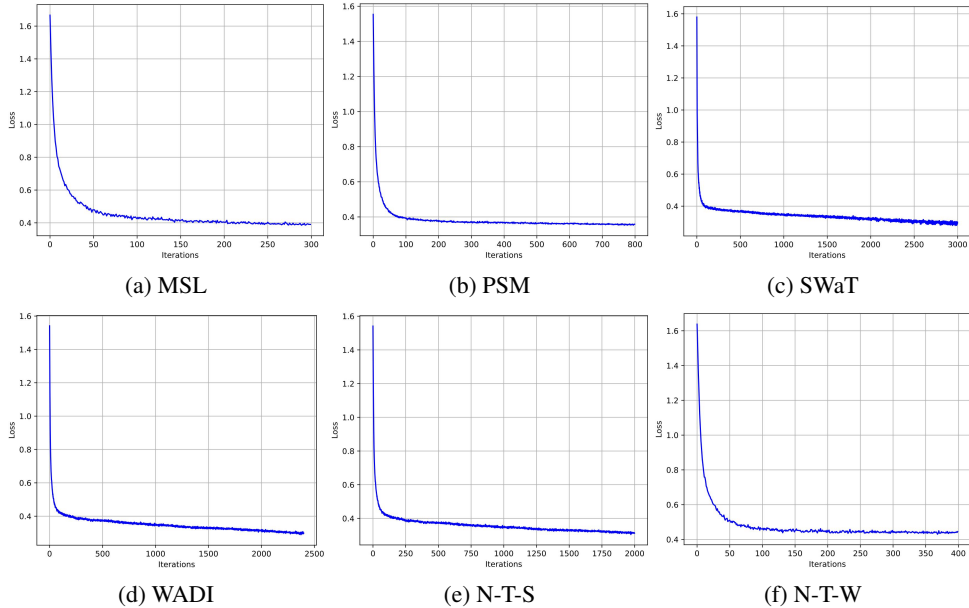


Figure 8: The convergence performance of our model’s loss on six different datasets is shown in the figure.

The convergence performance of the total loss (Equation 9) of our model on six different datasets is shown in the figure. Several consistent features can be observed from these curves: In all experiments, the loss function shows a similar convergence pattern, rapidly decreasing from an initial value of about 1.6 and gradually stabilizing. Specifically, within the first 100 iterations, the loss value drops rapidly to about 0.4, indicating that the model can effectively capture the key features of the data. Subsequently, the loss curve enters a gentle decline phase and converges to a stable value of about 0.3-0.4. It is worth noting that although the total number of iterations in each experiment is different (300, 800, 2000 and 3000 respectively), they all show similar convergence curve shapes, proving that the temporal topology constraint model we proposed has stable optimization characteristics and can effectively learn the main patterns of the data in a small number of iterations (about 100-200 iterations). This consistent convergence behavior further verifies the robustness and scalability of our model on different datasets.

J Run Times

To evaluate the practicality of ScatterAD in production environments, we comprehensively compared the training time, inference time, and GPU memory usage of various neural network models on the SWaT dataset. The results are shown in the table.

Table 14: Comparison of training time, inference time, and GPU memory consumption on the SWaT dataset.

Method	Training Time (s/iter)	Inference Time (s)	GPU Memory (GB)
GANF	0.177	0.834	8.202
DuoGAT	0.283	239.608	6.050
AnomalyTrans	0.378	86.134	12.424
MTGFlow	0.378	2.119	9.458
iTransformer	0.027	59.515	2.061
ModernTCN	0.012	59.882	1.923
DCdetector	0.012	59.882	1.923
MEMTO	0.621	8.582	19.91
TopoGDN	0.131	66.146	2.830
Sub-Adjacent Trans	0.107	1.762	5.396
ScatterAD	0.042	2.124	3.458

Table 14 reports the training and inference time per iteration, along with GPU memory usage on the SWaT dataset. Our method achieves the fastest training speed (**0.0421s/iter**). It also offers competitive inference efficiency and low GPU memory consumption. Compared to DuoGAT and Anomaly Trans, which suffer from extremely long inference times and high memory overhead, our model demonstrates superior scalability and deployment practicality.

K Limitations and Future Work

While ScatterAD shows strong performance across diverse real-world datasets, there remain a few avenues for future improvement. ScatterAD effectively captures spatial-temporal dependencies, and incorporating more explicit modeling of inter-series interactions may offer additional benefits in specialized applications such as industrial monitoring or financial forecasting. For future work, we aim to explore adaptive graph construction that evolves with streaming data to improve robustness in non-stationary environments. In addition, integrating causal discovery modules could enhance interpretability and detection precision. Another promising direction is extending ScatterAD to a semi-supervised or active learning setting, where limited anomaly labels can further guide representation learning.